The Architecture of a Complete Two-Component Signal Transduction System: Oxygen-Sensing Proteins FixL, FixJ, and the FixL-FixJ Complex

Gareth S. A. Wright,[1]† Akane Saeki,[2]† Takaaki Hikima,[3] Yoko Nishizono,[2] Tamao Hisano,[3] Misaki Kamaya,[2] Kohei Nukina,[2] Hideo Nishitani,[2] Hiro Nakamura,[3] Masaki Yamamoto,[3] Svetlana V. Antonyuk,[1] S. Samar Hasnain,[1] Yoshitsugu Shiro,[2,3]* Hitomi Sawai[2,3]*

[1]Molecular Biophysics Group, Institute of Integrative Biology, Faculty of Health and Life Sciences, University of Liverpool, Liverpool L69 7ZB, United Kingdom.
[2]Graduate School of Life Science, University of Hyogo, 3-2-1 Kouto, Kamigori, Ako, Hyogo 678-1297, Japan.
[3]RIKEN SPring-8 Center, 1-1-1 Kouto, Sayo, Hyogo 679-5148, Japan.

†These authors contributed equally to this work.
*Corresponding authors. E-mail: yshiro@sci.u-hyogo.ac.jp (Y.S.); sawai@sci.u-hyogo.ac.jp (H.S.)

Abstract

The symbiotic nitrogen-fixing bacterium, *Bradyrhizobium japonicum*, is critical to the agro-industrial production of soybean. Its FixL and FixJ two-component system (TCS) ensures that nitrogen fixation is stimulated under conditions of low oxygen. As a result of this symbiotic relationship and the activity of the FixL and FixJ TCS, it is possible to generate high yields of soybeans, which are globally important as staple foodstuffs, animal feed, and biofuel feedstock, with little use of nitrogenous fertilizers. We purified full-length *B. japonicum* FixL and FixJ proteins and defined their structures individually and in complex using small-angle X-ray scattering, crystallographic, and in silico modeling techniques. In this structural characterization of a complete TCS, comparison of active and inactive forms of FixL suggests that intra-molecular signal transduction is driven by local changes in the sensor domain and the coiled-coil region connecting sensor and histidine kinase domains. We also show that FixJ exhibits conformational plasticity not only in the monomeric state, but also in tetrameric complexes with FixL during phosphotransfer. This lends both a mechanistic and evolutionary understanding to TCS signal relay, specifically in the context of the control of root nodule nitrogen fixation.

Introduction

Two-component regulatory systems (TCSs) are widely distributed in bacteria, fungi, and higher plants. They facilitate cellular adaptation in response to environmental change. TCSs are considered to be good targets for the development of novel antibiotics and plant growth effectors because of their conspicuous absence in metazoans (*1-3*). TCSs are generally composed of two types of multi-domain proteins: sensory histidine kinases and response regulators. Class-I histidine kinases consist of an N-terminal stimulus-specific sensor domain and a C-terminal effecter module. The latter comprises the dimerization and histidine phosphotransfer (DHp) and catalytic ATP-binding (CA) domains. Response regulators contain a conserved N-terminal receiver (REC) domain, which is connected to diverse C-terminal effector domains. In response to an environmental stimulus sensed by the histidine kinase's sensor domain, the CA domain catalyzes the autophosphorylation of a specific histidine residue in the DHp domain. That phosphoryl group is subsequently transferred to a conserved aspartate residue in the REC domain of the cognate response regulator. This phosphotransfer activates the response regulator to promote DNA or RNA binding, enzymatic reactions, or protein interactions by the C-terminal effector domain (*4*).

The key questions of TCS signaling are how HKs are activated by stimuli and how the histidine kinase interacts with the response regulator. Answers to these questions have been hampered by the lack of molecular- and atomic-level structural information on intact, full-length histidine kinases in both the kinase-active and kinase-inactive forms and in complex with response regulators. To fill this dearth of knowledge, here we describe the structural characteristics of the oxygen (O_2)-sensing Fix L and Fix J TCS of the rhizobium species *Bradyrhizobium japonicum*, a root nodule, nitrogen-fixing bacterium that forms symbiotic relationships with leguminous plants such as soybean. FixL is a histidine kinase that senses the O_2 tension in the cytoplasm through a heme-containing PAS (Per-Arnt-Sim) domain and transfers phosphate from ATP by sequential autophosphorylation and phosphotransfer reactions in its C-terminal effector modules to the response regulator FixJ (Fig. 1). O_2 association to and dissociation from the heme-PAS domain of FixL trigger intra- and inter-molecular signaling mechanisms such that the deoxy (O_2-unbound) form of FixL is active for autophosphorylation and phosphotransfer, whereas its oxy (O_2-bound) form is inactive (*5*, *6*). As a result the rhizobial FixL and FixJ system stimulates the expression of genes required for nitrogen fixation only when O_2 concentrations in the plant root nodules are low, because the active center of nitrogenase is O_2-labile (*7*).

Although most TCS histidine kinases are integrated into the membrane for sensing extracellular stimuli, *B. japonicum* FixL is a water soluble, cytoplasmic sensor. The difficulty of purifying integral membrane TCS histidine kinases in combination with their multi-domain configurations and structural flexibility has inhibited structure-function studies. Thus, all previous structural studies of TCS histidine kinases, including FixL, were performed with truncated, rather than full-length, proteins. We have isolated full-length *B. japonicum* FixL and FixJ proteins at high purity and obtained structural information on Fix J, FixL in both the kinase-active (deoxy) and kinase-inactive (oxy) forms, and the FixL-FixJ complex by the combined use of the size-exclusion chromatography integrated small-angle X-ray scattering (SEC-SAXS), X-ray crystallography, and molecular modeling techniques. This analysis provides insights on how microorganisms and plants adapt to environmental change at the molecular level and elucidates details of a microbial signaling pathway that facilitates the agro-industrial production of human food, livestock feed, and biofuel with only limited need for nitrogenous fertilizers.

Results

Autophosphorylation and Phospho-Transfer Activities of Full-Length FixL and FixJ

We prepared recombinant full-length FixL and FixJ from *B. japonicum* with very high purity (fig. S1). *B. japonicum* FixL is a naturally occurring soluble FixL in contrast to some membrane anchored FixLs, for example, FixL from *Sinorhizobium meliloti*. *B. japonicum* FixL comprises N-terminal tandem PAS domains, PAS-A and PAS-B, followed by C-terminal DHp and CA domains (Fig. 1). The PAS-B domain senses O_2 through a heme *b* cofactor (*6*, *8*). The role of the N-terminal PAS-A domain in *B. japonicum* FixL is not clear, but some biological studies of the other water-soluble FixL from *Rhizobium etli* suggested that the PAS-A domain influences the oxygen affinity of the heme in the PAS-B domain (*9*).

We tested the phosphotransfer activity of our highly purified full-length FixL in several heme iron oxidation and ligation states. These included oxy (Fe^{2+}-O_2), deoxy (Fe^{2+}), ferric cyanide-bound (cyanomet; Fe^{3+}-CN^-) and ferric ligand-free (met; Fe^{3+}) forms (fig. S2). The phosphotransfer from FixL to FixJ was suppressed in the oxy and cyanomet forms, whereas the activities of these reactions were fully restored in the deoxy and met forms (Table 1). These results show that our preparation of full-length FixL and FixJ was successful, and that signal transduction by the FixL and FixJ system could be controlled by ligand (O_2 or CN^-) binding to the sensor domain of FixL, irrespective of the ferrous or ferric oxidation state of the heme iron. Due to the low affinity of O_2 for FixL (Table 1) and relatively fast autooxidation ($\tau_{1/2}$ ~ 15 min) of oxy FixL (*8*), we used the met and the cyanoment forms of the full-length FixL as analogues for the deoxy and oxy states, respectively, as samples for the SAXS measurements. We also found that, upon the CN^- binding to the heme iron of the FixL sensor domain in the met form, autophosphorylation activity was suppressed (fig. S3A), while the phosphatase activity was promoted (fig. S3B). Based on these experimental data, we expected that the tertiary and quaternary structures of full-length FixL are equivalent between ferric CN^- and ferrous O_2-bound forms.

Molecular Architecture of FixL

Very small amounts of aggregated protein can adversely affect SAXS measurements (*10*). Despite the high mono-dispersity of full-length *B. japonicum* FixL, small amounts of aggregation often resulted in poor SAXS data from static measurements (table S1). To overcome this effect, we performed SEC-SAXS, where the data collection was performed in-line with protein purification, both at the RIKEN beamline BL45XU (*11*) at the SPring-8 synchrotron in Japan and at the SWING beamline (*12*) at the SOLEIL synchrotron in France. The SEC chromatograms of FixL in the met form with SAXS parameters plotted together with absorbance at 280 and 398 nm clearly showed that the aggregated species were eliminated prior to the SAXS measurements (fig. S4A). Using this method, we measured SAXS from full-length FixL in the met and the cyanomet forms, and succeeded in obtaining data of high quality. The plot of log q vs log $I(q)$ obtained by SEC-SAXS at BL45XU (Fig. 2A), and the SEC-SAXS parameters are summarized in Table 2 and table S2. The data measured at SPring-8 and SOLEIL show a high degree of reproducibility. Radii of gyration (R_g) of 49.7±0.1 and 48.4±0.2 Å for met and cyanomet FixL respectively, are lower than those collected by static SAXS measurements (Table 2 and table S2), and reflect the ability of SEC-SAXS to isolate scattering from the species of interest. Molecular weight estimations from experimental SEC-SAXS data predict protein masses of 140.1±1.9 and 136.3±2.3 kDa, respectively, indicating that FixL in solution is in a homodimeric form. These observations are consistent with the structural characteristics of other histidine kinases, which have a stable four-helix bundle composed of two helices of the DHp domain from each monomer in the homodimer (*13*, *14*). The distance distribution function, $P(r)$, for each FixL state gave information on the maximum dimension (D_{max}) and the average electron distribution (Fig. 2B).

The D_{max} was calculated at 163±4 and 158±3 Å, respectively. CN^- binding to the heme group of FixL suppresses the kinase activity which is reflected in a slight decrease in R_g (48.4 Å vs 49.7 Å; Table 2) and D_{max} (163 Å vs 158 Å; Table 2).

Using the FixL SEC-SAXS data, it was possible to construct an *ab initio* model of full-length FixL in the met state. FixL exhibits an extended and club-like form (fig. S5). Correspondingly, dimensionless Kratky plot analysis of full-length FixL describes a protein, which does not adopt either a compact nor globular conformation (Fig. 2C). For comparison, we also measured its SEC-SAXS of a truncated form of FixL that contains only the PAS-A and PAS-B domains ($FixL_{PAS-PAS}$; Fig. 1 and fig. S6). Its Kratky plot is much different from that of full-length FixL and shows a high degree of globularity (Fig. 2C). Using this information as a guide, we constructed a pseudo-atomic model, of full-length FixL incorporating a combination of crystallographic domain structures, homology modelling, *a priori* structure prediction and refinement against the SAXS data. The constructed model is compared with the space filling model (Fig. 3A). The length of the dimer axis is identical to the experimentally determined D_{max} value (Table 2), and its calculated SAXS profile (fig. S7A) has a χ value of 2.57 when compared with the experimental data indicating the self-consistency of our proposed model and that it is a reasonable snapshot of FixL in solution.

Our model for FixL displays a tandem PAS domain forming homo-dimers (PAS A-A & PAS B-B), which are linearly connected to the DHp domain. There is no interaction between the PAS A dimer and the PAS B dimer or between either PAS A or B dimers and the CA domain. We note that the PAS-B sensor domain connects with histidine kinase module only through a coiled-coil linker region. This architecture of full-length FixL is comparable to an "in-line" model proposed for trans-membrane and membrane-associated histidine kinases (*13-15*).

Our constructed model has an asymmetric DHp domain (Fig. 3A). To test the possibility FixL has a symmetric four-helix bundle, we assembled models of FixL based on VicK (PDB: 4I5S, *16*), DesKC (PDB: 3GIE, *17*), CckA (PDB: 5IDJ, *18*) histidine kinases. This approach did not yield a better fit to the experimental data than provided by our proposed structure of intact, asymmetric full-length FixL (fig. S8).

Crystal and Solution Structures of FixJ

One of the most intriguing features of TCSs is the intermolecular communication that facilitate transfer of a phosphoryl group from histidine kinase to response regulator. We analyzed full-length FixJ alone with SEC-SAXS and crystallographic techniques. Crystallographic analyses showed three different conformers for FixJ, which was crystallized in space groups $C222_1$ and $P2_12_12_1$ (Figs. 4A & B and table S3). FixJ is a two-domain protein, comprising N-terminal α/β type REC domain with a phosphorylation site (Asp55), designated here as $FixJ_N$, and the C-terminal all α type effector domain with a helix-turn-helix DNA binding motif, $FixJ_C$. These two domains are connected by a helical linker. $FixJ_N$ exhibits the same fold as those reported for other N-terminal response regulator REC domains, and that of $FixJ_C$ exhibits characteristics of the C-terminal effector domain of the DNA-binding response regulator (*19*). The linker region contain two α-helices in the $C222_1$ data, the shorter of which (α6A) is conformationally flexible as shown by comparison of the three structures. Notably, helices α6A and α6B observed in the $C222_1$ data were fused to a single helix α6 in chains A–D of the $P2_12_12_1$ data, whereas helix α6A was transformed to a tight curve structure in the chain E of the $P2_12_12_1$ data. Structural comparison of the FixJ crystal structures with those of other full-length response regulators show that the α6A helix in the linker region is labile and acts as a hinge enabling response regulators in TCS including FixJ to have a variety of overall molecular shape.

The SEC-SAXS parameters of *B. japonicum* FixJ (Table 2), that is, R_g 22.3±0.2 Å, D_{max} 66±2 Å, molecular mass 24.5±0.7 kDa, are comparable with those for the *S. meliloti* orthologue (*20*), and indicate that FixJ in the un-phosphorylated state is a monomer in solution. An *ab initio* model

constructed from experimental scattering data showed that FixJ in solution exhibits an ellipsoidal shape (Fig. 4C and Table 2), and dimensionless Kratky plot analysis (Fig. 2C) also indicates that FixJ does not rest in an extended conformation in solution. No crystallographic conformer fitted the experimental SAXS data well, indicating that the average conformation of FixJ in solution is not fully represented by the crystal structures. We were able to refine the FixJ structure against the SAXS data to create a pseudo-atomic model that does fit the experimental data with χ value of 2.5 (Fig. 4D). In solution, $FixJ_N$ and $FixJ_C$ are able to fold back upon one another due to the kinked linking α-helix and allow a more compact structure. Indeed, the estimated D_{max} (66 Å) from the SAXS data is smaller than the longitudinal length of ~78 Å for a dumbbell-like shape of the crystal structures. This difference may arise from the conformational flexibility in the linker region, which confers conformation plasticity in solution.

Solution Structure of the Full-length FixL-FixJ Complex

To promote FixL-FixJ complex formation, we performed SEC of FixL in a buffer containing 40 μM FixJ. This concentration is 10-fold greater than the FixL-FixJ dissociation constant (K_d), which has been reported as 0.8 - 4.0 μM in the absence of ATP analogues and Mg^{2+} (*21*). Under this condition, the FixL-FixJ complex is expected to be predominant in solution. When the FixJ concentration in the loading buffer was reduced to 20 μM, the FixL-FixJ complex was not well separated from homodimeric FixL from by SEC.

The FixJ-saturated FixL elutes earlier than the FixL homodimer (Fig. S4B). Under these conditions, we collected SEC-SAXS data of FixL-FixJ complex in the met form (Fig. 2). Size parameters were found to be 53.1±0.1 Å for R_g, 160±5 Å for D_{max}, 185.4±1.5 kDa for molecular mass (Table 2). The R_g value was larger than that of FixL alone, and the molecular mass was increased by 45.3 kDa, indicative two molecules of FixJ (24.5 kDa) binding to FixL. These parameters indicate that phosphotransfer from FixL to FixJ is facilitated through homodimeric FixL binding to two FixJ molecules to form a heterotetramer. In addition, the SAXS data do not show large domain rearrangements on complex formation and dimensionless Kratky analysis (Fig. 2C) shows that the non-compact FixL conformation is conserved after complexation with two molecules of FixJ.

Based on this observation, we docked two FixJ monomers into our FixL pseudo-atomic model (Fig. 3B). In this construction, the 3-phospho-His^{291} in the FixL DHp domain and the phospho-acceptor Asp^{55} of the FixJ are within phosphotransfer distance (~3 Å). Overall fit of this model to the experimental SAXS data is good with χ of 2.71 (fig. S7B), validating the proposed model. To our knowledge, this is the first complete model of the complex formed by an intact full-length sensor histidine kinase and its full-length cognate response regulator that mediates TCS transduction.

To compare the kinase active FixL-FixJ complex with the inactive complex, we also measured the SEC-SAXS of the complex in the cyanomet form, whose parameters are shown in Table 2. Their values, especially R_g and D_{max}, were the same as those of the active met FixL-FixJ complex, suggesting that the ligand (CN^-) binding to the PAS-B sensor domain of FixL, which suppressed the kinase activity, does not strongly affect the overall molecular shape of the FixL-FixJ complex.

In the proposed FixL-FixJ complex, the $FixJ_N$ domains fit well within the SAXS envelope model, whereas the $FixJ_C$ domains do not. We hypothesize that, given the conformational flexibility of monomeric FixJ, the $FixJ_C$ domain is also able to adopt multiple conformations while in complex with FixL. Due to the dynamic nature of the linker region as observed in the crystallographic structure of FixJ (Fig. 4B). To test this possibility, we also measured and analyzed the SEC-SAXS of FixL complexed with $FixJ_N$. The SAXS parameters of the FixL-$FixJ_N$ complex showed that D_{max} (170±3 Å) is apparently similar to that of FixL-FixJ complex, while the molecular mass (153.6±1.4 kDa) and R_g (48.9±0.1 Å) values were smaller (Table 2). Absence of the $FixJ_C$ domain was reflected in mass and R_g, but gave no effect on the maximum dimension

of the FixL molecule. In addition, an *ab initio* model is not drastically different between FixL-FixJ and FixL-FixJ$_N$ complexes (Fig. S7B). These results suggest that, FixJ$_C$ does not contribute to the FixJ-FixL interaction and is instead free to move in solution.

Discussion

Intra- and inter-molecular signal transductions through the phosphoryl-transferring reactions of TCSs are ubiquitous for all living systems, except for animals. They allow adaptation to environmental changes with facilitates survival. To understand the molecular mechanism in detail, structural information of TCS histidine kinase, response regulator and their complex have been accumulated. However, many structural studies on TCSs have relied on breaking the protagonists down into tractable domains. Here, we have gained a structural understanding of a complete TCS; the full-length forms of *B. japonicum* O_2 sensing system, FixL, FixJ and FixL-FixJ complex. The information gained for the histidine kinase active and inactive forms of full-length FixL, and of full-length complex is particularly novel enabling us to comment on the modular structures that facilitate signal relay in this important TCS.

With respect to the intramolecular signal transduction from the sensor domain to the CA domain of the O_2 sensor protein FixL, two possible mechanisms have been proposed so far. Gonzales and co-workers proposed a "globular" model based on biochemical studies for the full-length *Rhizobium etli* FixL (*9*), which has a similar domain organization to *B. japonicum* FixL. In the *R. etli* FixL, interactions between two PAS dimers or between the PAS dimers and the CA domain for the globular formation are plausible. Therefore, it was proposed that changes to these interactions would be involved in the intra-molecular signal transduction stimulated by the O_2 association to or dissociation from the sensor PAS domain. On the other hand, the crystal structure of *Thermotoga maritima* ThkA, whose PAS domain exhibits 24 % primary structure similarity to that of FixL PAS-B, displays no interaction between the PAS domains, but rather direct interaction of the PAS domains with the CA domains through hydrogen bonding (*22*). The proposals were based on one assumption, that is, the mechanism of the intramolecular signal transduction is not necessarily similar between the water-soluble and membrane-integrated histidine kinases of TCS. The former HK works as a sensor of a stimulus in cytoplasm, while the sensor domain of the later histidine kinase senses an extracellular stimulus followed by transferring the information into the cytoplasm across the membrane for cellular adaptation (see below). However, the proposed architectures of *R. etli* FixL and the FixL analogue (ThkA) are incongruent with our present SAXS data of full-length *B. japonium* FixL, deduced parameters and low-resolution models. These structural inconsistencies suggest that neither the globular model nor the direct transfer of the signal from the sensor to the CA domains are possible.

Our results lead us to propose an "in-line" model for full-length FixL with dimerization through PAS A-A, PAS B-B and DHp interactions, but no direct interaction of the heme containing PAS-B domain with its CA domain (Fig. 3A). Our model of intact full-length FixL provides us with a structural basis, from which to discuss the molecular activation mechanism of autophosphorylation of TCS histidine kinase modules in response to stimuli. The full-length FixL met (active) and cyanomet (inactive) forms (Table 2) show that the overall molecular conformation is not largely changed upon activation. Correspondingly, our SAXS envelope models are also unaltered by CN^- binding (fig. S5A). Thus, it is likely that the conformational changes that control kinase activity following the ligand (CN^-) binding are localized, causing subtle changes in the interaction between the sensor domain and the CA domain. We propose that, upon O_2 dissociation from the heme iron in the PAS-B domain, a local conformational change in this domain, previously observed in FixL sensor domains (*23-27*), is propagated to the DHp

domain via the coiled-coil linker region. These structural changes cause ATP bound to the CA domain to come closer to the His^{291} residue of DHp, resulting in the phosphotransfer (Fig. 5).

To examine importance of the coiled-coil linker region in the FixL signal transduction from the sensor domain to the histidine kinase domain, we prepared 12 mutants of the coiled-coil region (R254A, T257A, E258A, E258Q, Q261A, T262A, T262S, Q263A, R265A, L266P, Q267A, L269P), and measured their phosphorylation activities in the met and cyanomet forms (fig. S9). As expected, their met forms were the kinase active, while the CN^--bound forms were inactive. Except for the E258Q mutant, which was tolerated and responded to the CN^- binding, the phosphorylation activities of the mutants in the met form were significantly reduced upon the mutation, suggesting that the dimerization in the coiled-coil region is responsible for activation of the kinase activities of histidine kinase module of FixL. In addition, it was also noted that the activity of R254A mutant showed 5-fold lower activity in the met form and modulate impairment of the CN^- responsiveness. Arg^{254} residues on the coiled-coil helices near the end of PAS-B domains might form a hydrogen bonding interact between the helices to regulate the activity upon CN^- binding. The results are apparently consistent with our previous work on preparation of chimeric sensor proteins, in which FixL PAS-B sensor domain was fused with histidine kinase of *T. maritima* ThkA at the coiled-coil region (*28*). The kinase activities of the chimeric proteins were impaired, maintained or unregulated by the ligand binding, depending on the fusing points. All these results support our proposal that the coiled-coil linker region between PAS-B and DHp domain works as a key modulator for the phosphorylation activity in FixL.

This proposal, the so-called “in-line” mechanism, is comparable to those given from previous studies for membrane-integrated or -associated histidine kinase of TCS such VicK and DesKC. The “truncated” structures of these histidine kinases, in which the transmembrane region and/or the extracellular domain were deleted (*14-18, 29*), were the basis of this proposal. However, there was no structural comparison between the kinase active and inactive forms of the histidine kinase in each TCS. One full-length structure of histidine kinase reported so far is an engineered and non-intact chimeric blue-light-regulated histidine kinase protein (YF1) (*30*), which was constructed by fusing the FixL histidine kinase module (DHp + CA domains) with the light sensing LOV domain of YtvA from *Bacillus subtilis*. On the basis of the structures of YF1, and of light-activated and inactive isolated LOV domain, it was suggested that the coiled-coil linker region between the sensor and the DHp domains promotes the symmetry and asymmetry transitions for the orientation of the DHp and the CA domains. Here, it was noted the mutagenesis results of the coiled-coil linker region of YF1 are comparable to those of FixL (fig. S8). Therefore, our present study using the intact and full-length FixL establishes the intramolecular signal transducing mechanism of histidine kinase.

Autophosporylation of His^{291} in the FixL DHp domain is followed by the phospho-transfer reaction, in which the phosphoryl group is transferred to Asp^{55} of the $FixJ_N$. Formation of a transient FixL-FixJ complex facilitates phosphotransfer. To gain insight into this transient state in solution, we collected SEC-SAXS data under FixJ-saturated conditions, and observed SAXS parameters indicating the FixL and FixJ complex stoichiometry of 2:2. This result is consistent with a handful of structural data for truncated histidine kinase and truncated response regulator complexes: HK853-RR468 (*15*), ThkA-TrrA (*22*), DesK-DesR (*17*) and Spo0B-Spo0F (*29*). Shimizu and co-workers recently reported that *Af*GcHK and its cognate response regulator predominantly form a complex with 2:1 stoichiometry (*31*), however we could not obtain the 2:1 complex under excess condition of response regulator by our SEC-SAXS study.

Our SAXS data indicate that FixJ binding induces no drastic FixL conformation change (Figs. 4A and B). This observation is consistent with previous crystallographic studies of the truncated histidine kinase and response regulator complex shown above (*15, 17, 29*), in which a slight rotation of the CA domain was observed, but any drastic change of the overall structures was not

(Fig. 5). In addition, volume associated with the $FixJ_N$ REC domain is present close to the DHp-CA regions of the space filling model (Fig. 3B). Since the phosphortransfer reaction from histidine kinase to response regulator is common in the TCS physiological action, such specific recognition and association of the REC domain by the histidine kinase observed in the full-length FixL-FixJ complex are unambiguously general features of TCSs. Following activation by phosphotransfer to the Asp residue in the REC domain of response regulator and release from the histidine kinase, the C-terminal effector domain of response regulator dimerizes and then interacts with its specific target. FixJ phosphorylation promotes the expression of NifA and FixK genes by binding to upstream elements. This in turn promotess transcription from over 100 genes including the nif and fix gene clusters which code for nitrogen fixation proteins. The function of the response regulator is highly variable and can be DNA-binding (69.4 %), RNA-binding (1 %), protein-binding (1.7 %) or an integral enzymatic activity (8.1 %) (*32*). Such functional diversity is reflected in the structural diversity of the C-terminal effector domain of response regulator. There are at least 35 classes of RR. Each class can contain anywhere from one protein up to roughly 25,000 (*32, 33*). It appears to us that a conformationally flexible response regulator, as described here for FixJ, very effectively limits the role of the effector domain in complexation with the histidine kinase (Fig. 5). This is necessary to ensure that structurally disparate effector domains can be activated by a general TCS phosphotransfer mechanism to the REC domain of response regulator. Thus, modularity ensures functionality.

The O_2 sensor FixL-FixJ system examined in this study is categorized as a class-I histidine kinase, where the DHp domain is directly adjacent to the CA domain (*34*, *35*). Although all histidine kinase discussed here such as VicK, DesK, CckA, EnvZ, HK853, and ThkA are fall into the same category, the domain architecture of FixL is the simplest among them. On the other hand, FixJ belongs to the NarL-like superfamily, consisting of a REC and a helix-turn-helix DNA binding domain (effector domain) as a transcriptional regulator (*36*), which is the largest family of response regulators. For the class-I histidine kinases, the REC domain is a common component to receive a phosphate group. Therefore, the full-length architecture of the FixL-FixJ system expected to suggest the general mechanism of intra- and inter-molecular signal transduction in class-I histidine kinase and response regulator of TCS, in which the so-called “in-line” mechanism is possible, irrespective to water-soluble (cytosolic) and membrane-integrated histidine kinase sensors, and that the effector domain of response regulator ($FixJ_C$ domain in the case of FixJ) in the complex does not interact with histidine kinase. In addition, the present study would provide fundamental knowledge for understanding the physiological, biochemical and biological importance of TCS, in particular class-I category, including their molecular evolution (*37*) or protein engineering for synthetic biological system for antibiotic and plant growth effector development.

The rhizobia are a group of nitrogen fixing bacteria that are proficient at establishing symbiotic relationships with leguminous plants; a global staple food group. This relationship provides nitrates to the host and a boost to growth and plant survival with benefits to agricultural productivity. The model organism *B. japonicum* is of particular interest in this regard because it resides in the root nodules of the soybean plant, *Glycine max*, which provides more protein per hectare cultivated than any other food source. Indeed, *B. japonicum* is sprayed onto soybean seed stock on an industrial scale to take advantage of this relationship. Our results open the path for genetic modification of this Rhizobial TCS to improve crop yields.

Materials and Methods

Preparation of recombinant FixL and FixJ proteins

Bradyrhizobium japonicum FixL and FixJ genes not only for full-length but also FixL truncation ($FixL_{PAS\text{-}PAS}$, residues 1-275) and $FixJ_N$ (residues 1-124) were separately amplified by PCR with PfuTurbo DNA polymerase (Agilent technologies). The PCR fragments were cleaved by *Bsr*GI and *Avr*II for FixL, *Bsr*GI and *Nhe*I for FixJ (New England Biolabs), and cloned into 5'*Bsr*GI-3'*Avr*II sites of pET-47b(+) vector (Novagen). Site-directed mutagenesis of the coiled-coil region in full-length FixL was performed by QuikChange protocol using pET-47b(+) vector inserted the full-length FixL gene as a template.

E. coli BL21(DE3) cells (Nippon gene) carrying these plasmids were inoculated in TB broth containing 50 μg/mL kanamycin (Wako) and 1% glucose for 4 hours at 37 ºC with shaking at 150 rpm. 1 mL of the preculture solution was inoculated into 300 mL TB medium containing 50 μg/mL kanamycin [and 250 μM 5-aminolevulinic acid (Cosmo energy holdings) only for the expression of FixL]. The cultivation was done at 37 ºC with shaking at 120 rpm. After 4 hours of the cultivation, expression of FixL or FixJ was induced with 0.3 or 0.2 mM isopropyl-β-D-thiogalactopyranoside, respectively, and cultivation allowed to continue for another 15 hours at 23 ºC with shaking at 80 rpm. The cells were harvested by centrifugation at 4,000 x g for 10 min., and the cells were washed in 30 mM Tris/HCl (pH8.0) twice.

Purification of FixL and FixJ was performed by the following same steps at 4 ºC. Harvested cells were resuspended in a lysis buffer [50 mM Tris/HCl pH8.0, 300 mM NaCl, 10% w/v glycerol, 1 tablet of cOmplete EDTA-free protease inhibitor cocktail (Roche)]. The lysate was mixed with 0.1 mg/mL lysozyme (Sigma-aldrich), 0.05 mg/mL DNaseI (Sigma-aldrich) and 5 mM $MgCl_2$ for 30 min., and disrupted by Microfluidizer® M-110Y (Microfluidics). Cell debris was removed by ultracentrifugation at 40 krpm for 1hour. The supernatant was loaded to His-Trap HP (GE healthcare) equilibrated with buffer-A (50 mM Tris/HCl pH8.0, 300 mM NaCl, 10% w/v glycerol, 10 mM imidazole/HCl pH8.0). FixL or FixJ was eluted by an imidazole concentration gradient (0-300 mM). The eluted fractions were added N-terminal 6xHis-tag fused HRV3C protease (in-house production) to cleavage 6xHis-tag, and the solution was dialyzed with buffer-B (40 mM Tris/HCl pH8.0, 150 mM NaCl, 10% w/v glycerol). After the dialysis, the protein solution was loaded to His-Trap FF (GE healthcare) equilibrated with buffer-B to remove the HRV3C protease and His-tag remaining proteins, and the flow through was collected. The collected solution was concentrated by AmiconUltra-15 (Merck Millipore), and centrifuged at 15 krpm for 20 min. The supernatant was loaded to HiLoad 16/600 Superdex 200 (GE healthcare) equilibrated with buffer-B. The purity of FixL or FixJ was checked by 10% SDS-PAGE. In FixL, the highly purified fractions showed Rz (A_{398nm}/A_{280nm}) value > 1.3 used for SAXS studies. Because His-tagged full-length FixL showed the activity regulation upon cyanide binding to the heme and almost the same levels of phosphotransfer activity with His-tag-removed protein, we used the His-tagged full-length FixL proteins on the phosphorylation activity assay of the coiled-coil mutants (fig. S9).

Autophosphorylation, phosphotransfer, and phosphatase activity assay of purified FixL and FixJ proteins

Autophosphorylation of FixL protein was monitored by radioactivity of phosphorylated FixL by ^{32}P. Reaction mixtures contained 2 or 6 μg FixL in 7.5 μL of 50 mM Tris/HCl pH8.0, 50 mM KCl, 1 mM $MgCl_2$, 50 μM $MnCl_2$, 5% w/v glycerol with or without 5 mM KCN. The reactions were started with the addition of the mixture of ATP (10 or 25 nM) and γ-^{32}P-ATP (4 or 10 μCi) (PerkinElmer). Incubated the reaction mixture at 23ºC for 10 min., and stopped with one-fourth volume of SDS-PAGE sample buffer. After SDS-PAGE, phosphorylated proteins were measured on an imaging plate.

Phosphotransfer activities from FixL to FixJ were determined using an enzymatic assay in which ATP hydrolysis is coupled to NADH oxidation using lactate dehydrogenase and pyruvate kinase (*38*). To measure basal activity, the reaction buffer [50 mM Tris/HCl pH8.0, 50 mM KCl, 3 mM phosphoenolpyruvic acid (Wako), 0.3 mM NADH (Sigma-aldrich), 8 units lactate dehydrogenase (Toyobo), 25 units pyruvate kinase (Sigma-aldrich), 5 mM $MgCl_2$, 5 mM ATP] was equilibrated at 20ºC for 5 min. The reaction was started by the addition of 1 μM purified FixL and 10 μM purified FixJ, and the time course of A_{340nm} was monitored for 10 min at 20ºC. An NADH standard curve with a range of NADH concentrations between 0 and 150 μM was measured in the same buffer. To measure the activity of cyanomet form, 5 mM KCN was added to the reaction buffer before the addition of FixL protein.

Phosphatase activity of FixL was monitored the dephosphorylation of acetylphosphorylated FixJ by unphosphorylated FixL. The acetylphosphate-dependent FixJ autophosphorylation was performed in 50 mM Tris/HCl pH8.0, 50 mM KCl, 1 mM $MgCl_2$, 50 μM $MnCl_2$, 20 μM FixJ, and 50 mM acetyl phosphate lithium potassium salt (Sigma-aldrich) at 23 ºC. After 2hours, unphosphorylated FixL (10 μM, wild-type) was added to the reaction mixture. The incubation times for the reactions were 0 (before FixL addition), 5, 15, 30, 60, and 120 mins after the addition of the FixL. The reactions were stopped with two-third volume of SDS-PAGE sample buffer. The reaction products were subjected to 15% Zn^{2+}-Phos-tage SDS-PAGE containing 50 μM Phos-tag® acrylamide (Wako) and 100 μM $ZnCl_2$, the gel was stained by EzStain AQua (ATTO).

SEC-SAXS data collection and analysis

SEC-SAXS data collection was performed at RIKEN beamlines BL45XU (*11*) in SPring-8 and at beamline SWING (*12*) in the French national synchrotron SOLEIL. At BL45XU in SPring-8, the purified protein was loaded onto a Superdex200 Increase 3.2/300 (GE healthcare) in a 20 μL volume at 50 μL/min flow rate with a SEC buffer [40 mM Tris/HCl pH8.0, 10%(w/v) glycerol, 5 mM $MgCl_2$] at 20 ºC. For the data collection of cyanomet FixL, 5 mM KCN was added to the SEC buffer, and the loading FixL sample was mixed with KCN at the final concentration of 5 mM. For the detection of FixL-FixJ complex or FixL-$FixJ_N$ complex, saturating amount of FixJ or $FixJ_N$ (more than 10 times of the K_d value)-containing SEC buffer used to improve the affinity of FixL and FixJ. X-ray exposure was 1 sec every 4 sec with the incident beam energy 12.4 keV. 30 x 1 sec buffer frames were averaged and subtracted from 30 x 1 sec frames taken over the course of protein elution. The sample-detector distance was 2 m giving an angular momentum transfer range of q_{min} = 0.009 $Å^{-1}$ to q_{max} = 0.5 $Å^{-1}$. The flux density was about 2 x 10^{12} photons/sec/mm. Scattering was collected on a PILATUS 3X 2M detector (DECTRIS). Data averaging and reduction were calculated by the program DataProcess installed in BL45XU. Measurements at SWING were performed as above but using an Agilent BioSEC-3 4.6×300 mm column (Agilent) with 3 μm bead size and 300 Å pore size at 15ºC after double purification on a Superdex200 Increase 10/300 (GE healthcare) at 4ºC. Beam energy was 12 keV and sample detector distance was 1.8 m.

R_g and I_0 calculations on SEC-SAXS data were performed with AutoRg. Data of interest was averaged and the Guinier estimation performed in Matlab and PRIMUS (*39*) (fig. S10). Distance distribution functions $P(r)$ were calculated with GNOM (*40*) and ScÅtter based on agreement between real and reciprocal space R_g values (<3% difference) and fit to the experimental data. This was performed independent of crystallographic and homology model building. Bead models were generated with DAMMIN (*41*).

Crystallization, data collection, and refinement for the full-length FixJ structure

Crystals of FixJ in space group $C222_1$ (Form 1) were obtained at 20˚C by vapour diffusion using a mother liquor containing 10%(w/v) PEG8000, 10%(w/v) PEG1000, 0.8 M sodium

formate, 20%(v/v) glycerol, and 0.1 M Tris-HCl (pH 7.5). The asymmetric unit contained one polypeptide chain. Crystals of FixJ in space group $P2_12_12_1$ (Form 2) were obtained at 20˚C by vapour diffusion using a mother liquor containing 20%(w/v) pentaerythritol ethoxylate (15/4 EO/OH), 0.1 M magnesium formate, 20%(v/v) glycerol, and 0.1 M Tris-HCl (pH 8.5). The asymmetric unit contained five polypeptide chains. Crystals of both forms were grown in three days, and frozen and stored in liquid nitrogen. Data collection was carried out at BL26B2 in SPring-8, Harima, Japan (*42, 43*), equipped with an automated sample mounting system (*44*). Crystals were cryo-cooled in a nitrogen gas stream at 100K during data collection. The data were integrated and scaled using HKL2000 (*45*). Initial phases for the data set of the crystal form 1 were obtained by molecular replacement using coordinates of StyR (PDB ID: 1YIO) (*46*) as a search model in PHENIX (*47*). The coordinates of the N- and C-terminal domains of StyR were extracted and used for the molecular replacement calculation, because the structure of the linker region may vary from protein to protein in the response regulator family. Initial phases were used for model building, and improved by refinement of the model coordinates, including model building of the linker domain, in PHENIX (*47*) and COOT (*48*). The final model included residues from 2 to 203, and four glycerols, six formic acids and 257 water molecules. Initial phases for the data set of the crystal form 2 were obtained by molecular replacement using coordinates of the form 1 structure in PHENIX, with the N- and C-terminal domains separated. Four solutions for each domain were obtained, and used for model rebuilding and refinement including the linker regions (chains A – D) in PHENIX and COOT. During refinement, weak but continuous densities appeared in solvent region. Lowering the contour level revealed the fifth molecule for the densities. Each separated copy of the models of the three domains was manually fitted in the electron densities (chain E). Coordinates of the five polypeptide chains were further refined including magnesium ions and water molecules. The final model included 1,015 residues, four magnesium ions, and eight glycerols, seven formic acids, and 163 water molecules. Model quality was checked by MOLPROBITY (*49*) in PHENIX.

Pseudo-atomic model building and refinement against SAXS data

Jpred (*50*) and Coils (*51*) were used to ascertain which parts of the FixL sequence form α-helices and coiled coils. The structure of the blue light receptor (PDB ID: 4GCZ) was used as a model for the histidine kinase domain and the alpha helices beyond Thr257. This was linked to the structure of FixL heme-PAS domain (PDB ID: 1DRM). The coiled-coil helix N-terminal of the heme-PAS to the PAS-A domain was created with PEP-FOLD (*52*). This was linked to a homology model of the PAS-A domain created from a sensory histidine kinase from *B. thailandensis* (PDB ID: 3MR0). The cloning fragment from pET-47b(+) vector (10 amino acid residues, GPGYQDPNSV) was also constructed using PEP-FOLD. This initial structure had χ^2 3.93 against experimental data calculated using FoXS (*53*). Torsion angle molecular dynamics (MD) in CNS (*54*) was used to refine the positions of domains and loops in this structure against SAXS data as described in Wright et al 2016 (*55*). To validate the region of the model encompassing amino acids 1-256 which was assembled from a crystal structure, a homology model and several *ab initio* structure predictions we created a FixL 1-275 truncation including cloning fragment and measured SAXS. This data was exceptionally congruent with the PAS A-PAS B part of our FixL model indicating the proposed domain arrangement and interfaces are correct. The chimeric sensor protein structure 4GCZ shows structural asymmetry possibly resulting from crystal packing or partial ADP binding. We created three models of FixL based on VicK, DesKC, and CckA histidine kinases, each of which have symmetric four helix bundles, based on their coverage of and identity to FixL amino acids 258-505. Homology models were generated with SWISS-MODEL in conjunction with the method above and HADDOCK (*56*) to refine and dock the ADP-free CA domains in order to find an optimum ADP-free structure. This

pool of structures has consistently worse fit to our experimental data than that based on 4GCZ indicating that FixL adopts an asymmetric conformation in solution in the ADP-free state.

The structures of FixJ were refined against SAXS data using the torsion angle MD process described above. We initially defined the location of FixJ binding to FixL using pyDOCKSAXS (*57*) and FoXSDOCK (*58*). These programs use a combination of FTDOCK/Crysol and PatchDock/FoXS to assign interactions. Using this approach, and without defining the FixL His^{291}-FixJ Asp^{55} interaction site, FixJ was consistently positioned on the FixL four helix bundle. FixJ receiver domains were then directed to FixL His^{291} on both chains using HADDOCK. The FixJ linkers and DNA binding domains were then added based out SAXS refined structure of the FixJ monomer. The positions of these latter domains were then determined using CNS torsion angle MD. Trimeric complexes of dimeric FixL with one FixJ monomer were also constructed and optimized by torsion angle MD/rigid body refinement but were found to consistently produce models that fit the data poorly in comparison with the tetrameric architecture.

Supplementary Materials

fig. S1. SDS-PAGE of purified FixL and FixJ samples.
fig. S2. Optical absorption spectra of full-length FixL in oxy, deoxy, met and cyanomet forms.
fig. S3. Autophosphorylation and phosphatase activity assay.
fig. S4. SEC profiles.
fig. S5. Space filling models of FixL and FixL-FixJ complex.
fig. S6. Experimental and simulated SAXS curves of FixL in the met and FixL-FixJ complex.
fig. S7. Pseudo-atomic model and SAXS curve of truncated FixL ($FixL_{PAS\text{-}PAS}$).
fig. S8. SAXS curves and pseudo-atomic models of full-length FixL based on the YF1 blue light receptor compared with other models based on symmetric DHp domain structures.
fig. S9. Phosphorylation activities of FixL mutants on the coiled-coil region between PAS-B and DHp domains.
fig. S10. Guinier plots with Pearson residuals on SEC-SAXS measurements.
table S1. Structural parameters for FixL and FixJ determined by static SAXS experiments at BL45XU in SPring-8.
table S2. Structural parameters for FixL, FixJ, and FixL and FixJ complex by SEC-SAXS experiments at SWING beamline in SOLEIL.
table S3. Crystallographic statistics of FixJ.

Figure Legends

Fig. 1. Schematic representation of the domain structures of full-length and truncated versions of *B. japonicum* FixL and FixJ. Full-length *B. japonicum* FixL comprises two N-terminal PAS domains, PAS-A and PAS-B, and C-terminal dimerization and histidine phosphotransfer (DHp) and catalytic ATP-binding (CA) domains. His^{200} in the PAS-B domain is critical for binding to heme; His^{291} in the DHp domain is the site of autophosphorylation; and Asp^{431}-Val^{467} of the CA domain constitutes the ATP binding site. Full-length *B. japonicum* FixJ contains an N-terminal receiver (REC) domain and a C-terminal effector domain that binds to DNA. FixJ is activated by FixL-mediated phosphorylation at Asp^{55}. Structures of the truncated FixL and FixJ proteins $FixL_{PAS\text{-}PAS}$ and $FixJ_N$ used in this study are indicated. The residues that define the boundaries of these domains are noted. Domain structures were generated using the SMART tool (http://smart.embl-heidelberg.de/).

Fig. 2. SEC-SAXS profiles of full-length FixL, FixJ, and FixL-FixJ complexes. (**A**) Log-log plots of met and cyanomet forms of full-length FixL, full-length FixJ, the FixL-FixJ complex, and the FixL-$FixJ_N$ complex scattering. (**B**) Corresponding pair distance distribution functions. (**C**) Dimensionless Kratky plots, which compare the compactness of a protein, for full-length FixL (met form), truncated $FixL_{PAS-PAS}$ form of FixL (met form), full-length FixJ, and the full-lengths FixL and FixJ complex. A compact protein has a peak maximum at √3 and 1.2. Movement of the peak into the positive quartile indicates unfolding and conformational flexibility. Data was collected on the BL45XU beamline at the SPring-8 synchrotron. N>3 from independent protein preparations and data collections.

Fig. 3. Space filling and pseudo-atomic models of full-length FixL and the FixL-FixJ complex. SAXS models of (**A**) the met form of full-length FixL and (**B**) the FixL-FixJ complex showing the overall shape, domain arrangement and mode of complexation. The $FixJ_C$ effector domain is invisible in the *ab initio* model of the FixL-FixJ complex because it does not form part of the complex interface and is allowed conformational freedom by its inter-domain linker as characterized in Fig. 4.

Fig. 4. Crystal and SAXS solution structures of full-length FixJ. (**A**) Crystal structure of full-length FixJ showing the relative positions of the N-terminal (pink), linker (cyan), and C-terminal (green) domains. The phosphorylation site, Asp^{55}, is indicated as a stick model (carbon and oxygen atoms are indicated in yellow and red, respectively). (**B**) Comparison of crystal structures of FixJ in space groups $C222_1$ (blue) and $P2_12_12_1$ [yellow (chain A) and magenta (chain E)]. This view is rotated by 90^o compared to (A). (**C**) Space filling and pseudo-atomic models of full-length FixJ. (**D**) Comparison of FixL crystallographic and SAXS models against experimental SAXS data.

Fig. 5. Schematic representation of of the FixL/FixJ TCS. Our SAXS results suggest that there are no large overall changes of the shape of full-length FixL upon O_2 dissociation from the heme group. However, the orientation of the coiled-coil helices between the heme-containing PAS-B (pink) and DHp (green) domains may change. Such localized structural change could alter the distance between the ATP binding site in the CA domain (orange) and the autophosphorylation site at His^{291}. In the full-length FixL-FixJ complex, a phosphorylation site (Asp^{55}) in the FixJ REC domain approaches to the His^{291} of the FixL DHp domain, while the C-terminal DNA binding domains of FixJ exhibit multiple-conformation due to flexible linker conformation.

References and Notes

1. T. Urao, K. Yamaguchi-Shinozaki, K. Shinozaki, Two-component systems in plant signal transduction. *Trends in Plant Sci.* **5**, 67-74 (2000).
2. Y. Gotoh, Y. Eguchi, T. Watanabe, S. Okamoto, A. Doi, T. Utsumi, Two-component signal transduction as potential drug targets in pathogenic bacteria. *Curr. Opin. Microbiol.* **13**, 232-239 (2010).
3. N. Chauhan, R. Calderone, Two-component signal transduction proteins as potential drug targets in medically important fungi. *Infect. Immun.* **76**, 4795-4803 (2008).
4. R. Gao, A. M. Stock, Biological insights from structures of two-component proteins. *Annu. Rev. Microbiol.* **63**, 133-154 (2009).

5. M. A. Gilles-Gonzalez, G. S. Ditta, D. R. Helinski, A heamoprotein with kinase activity encoded by the oxygen sensor of *Rhizobium meliloti*. *Nature* **350**, 170-172 (1991).

6. W. Gong, B. Hao, S. S. Mansy, G. Gonzalez, M. A. Gilles-Gonzalez, Structure of a biological oxygen sensor: a new mechanism for heme-driven signal transduction. *Proc. Natl. Acad. Sci. USA* **95**, 15177-15182 (1998).

7. M. David, M. Daberan, J. Batut, A. Dedieu, O. Domergue, J. Ghai, C. Hertig, P. Boistard, D. Kahn, Cascade regulation of *nif* gene expression in *Rhizobium meliloti*. *Cell* **54**, 671-683 (1988).

8. M. A. Gilles-Gonzalez, G. Gonzalez, N. F. Perutx, L. Kiger, M. C. Marden, C. Poyart, Heme-based sensors, exemplified by the kinase FixL, are a new class of heme protein with distinctive ligand binding and autoxidation. *Biochemistry* **33**, 8067-8073 (1994).

9. E. H. S. Sousa, J. R. Tuckerman, A. C. S. Gondim, G. Gonzalez, M. A. Gilles-Gonzalez, Signal transduction and phosphoryl transfer by a FixL hybrid kinase with low oxygen affinity: importance of the vicinal PAS domain and receiver aspartate. *Biochemistry* **52**, 456-465 (2013).

10. G. S. Wright, Hasnain, S. S., Grossmann, J. G. (2011) The structural plasticity of the human copper chaperone for SOD1: insights from combined size-exclusion chromatographic and solution X-ray scattering studies. *Biochem. J.* 439(1):39-44.

11. T. Fujisawa, K. Inoue, T. Oka, H. Iwamoto, T. Uruga, T. Kumasaka, Y. Inoko, N. Yagi, M. Yamamoto, T. Ueki, Small-angle X-ray scattering station at the SPring-8 RIKEN beamline. *J. Appl. Chrystllogr.* **33**, 797-800 (2000).

12. G. David, J. Pérez, Combined sampler robot and high-performance liquid charomatography: a fully automated system for biological small-angle X-ray scattering experiments at the Synchrotron SOLEIL SWING beamline. *J. Appl. Cryst.* **42**, 892-900 (2009).

13. M. P. Bhate, K. S. Molnar, M. Goulian, W. F. DeGrado, Signal transduction in histidine kinases: insights from new structures. *Structure* **23**, 981-994 (2015).

14. P. Casino, V. Rubio, A. Matina, The mechanism of signal transduction by two-component systems. *Curr. Opin. Struct. Biol.* **20**, 763-771 (2010).

15. P. Casino, V. Rubio, A. Marina, Structural insight into partner specificity and phosphoryl transfer in two-component signal transduction. *Cell* **139**, 325-336 (2009).

16. C. Wang, J. Sang, J. Wang, M. Su, J. S. Downey, Q. Wu, S. Wang, Y. Cai, X. Xu, J. Wu, D. B. Senadheera, D. G. Cvitkovitch, L. Chen, S. D. Goodman, A. Han, Mechanistic insights revealed by the crystal structure of histidine kinase with signal transducer and sensor domains. *PLoS Biol.* **11**, e1001493 (2013).

17. F. Trajtenberg, J. A. Imelio, M. R. Machado, N. Larrieux, M. A. Marti, G. Obal, A. E. Mechaly, A. Buschiazzo, Regulation of signaling directionality revealed by 3D snapshots of a kinase: regulator complex in action. *eLife* **5**, e21422 (2016).

18. B. N. Dubey, C. Lori, S. Ozaki, G. Fucile, I. Plaza-Menacho, U. Jenal, T. Schirmer, Cyclic di-GMP mediates a histidine kinase/phosphatase switch by noncovalent domain cross-linking. *Sci. Adv.* **2**, e1600823 (2016).

19. A. Doi, H. Nakamura, Y. Shiro, H. Sugimoto, Structure of the response regulator ChrA in the haem-sensing two-component system of *Corynebacterium disphtheriae*. *Acta Crystallogr. F Struct. Biol. Commun.* **71**, 966-971 (2015).

20. C. Brick, M. Malfois, D. Svergun, J.-P. Samama, Insights into signal transduction revealed by the low resolution structure of the FixJ response regulator. *J. Mol. Biol.* **321**, 447-457 (2002).

21. E. H. S. Sousa, G. Gonzalez, and M. A. Gilles-Gonzalez, Oxygen blocks the FixL-FixJ complex with ATP but does not influence binding of FixJ or ATP to FixL. *Biochemistry* **44**, 15359-15365 (2005).

22. S. Yamada, H. Sugimoto, M. Kobayashi, A. Ohno, H. Nakamura, Y. Shiro, Structure of PAS-linked histidine kinase and the response regulator complex. *Structure* **17**, 1333-1344 (2009).

23. W. Gong, B. Hao, M. K. Chan, New mechanistic insights from structural studies of the oxygen-sensing domain of *Bradyrhizobium japonicum* FixL. *Biochemistry* **39**, 3955-3962 (2000).

24. C. M. Dunham, E. M. Dioum, J. R. Tuckerman, G. Gonzalez, W. G. Scott, M. A. Gilles-Gonzalez, A distal arginine in oxygen-sensing heme-PAS domains is essential to ligand binding, signal transduction, and structure. *Biochemistry* **42**, 7701-7708 (2003).

25. J. Key, K. Moffat, Crystal structure of deoxy and CO-bound *Bj*FixLH reveal details of ligand recognition and signaling. *Biochemistry* **44**, 4627-4635 (2005).

26. V. Balland, L. Bouzhir-Sima, L. Kiger, M. C. Marden, M. H. Vos, U. Liebl, Role of arginine 220 in the oxygen sensor FixL from *Bradyrhizobium japonicum*. *J. Biol. Chem.* **280**, 15279-15288 (2005).

27. V. Balland, L. Bouzhir-Sima, E. Anzolabéhère-Mallart, A. Boussac, M. H. Vos, U. Liebl, Functional implications of the propionate 7-arginine 200 interaction in the FixLH oxygen sensor from *Bradyrhizobium japonicum*. *Biochemistry* **45**, 2072-2084 (2006).

28. H. Kumita, S. Yamada, H. Nakamura, Y. Shiro, Chimeric sensor kinases containing O_2 sensor domain of FixL and histidine kinase domain from thermophile. *Biochim. Biophys. Acta* **1646**, 136-144 (2003).

29. J. Zapf, U. Sen, Madhusudan, J. A. Hoch, K. I. Varughese, A transient interaction between two phosphorelay proteins trapped in a crystal lattice reveals the mechanism of molecular recognition and phosphotransfer in signal transduction. *Structure* **8**, 851-862 (2000).

30. R. P. Diensthuber, M. Bommer, T. Gleichmann, A. Möglich, Full-length structure of a sensor histidine kinase pinpoints coaxial coiled coils as signal transducers and modulators. *Structure* **21**, 1127-1136 (2013).

31. M. Stranave, V. Martinek, P. Man, V. Fojtikova, D. Kavan, O. Vanek, T. Shimizu, M. Martinkova, Structural characterization of the heme-based oxygen sensor, *Af*GcHK, its interactions with the cognate response regulator, and their combined mechanism of action in a bacterial two-component signaling system. *Proteins* **84**, 1375-1389 (2016).

32. C. P. Zschiedrich, V. Keidel, H. Szurmant, Molecular mechanisms of two-component signal transduction. *J. Mol. Biol.* **428**, 3752-3775 (2016).

33. M. Y. Galperin, Diversity of structure and function of response regulator output domains. *Curr. Opin. Microbiol.* **13**, 150-159 (2010).

34. C. Tomomomori, H. Kurokawa, M. Ikura, The histidine kinase family: structures of essential building blocks. in *Histidine kinases in signal transduction* (eds. M. Inoue and R. Dutta) 12-14, Academic Press, New York (2003).

35. R. Dutta, L. Qin, M. Inouye, Histidine kinases: diversity of domain organization. *Mol. Microbiol.* **34**, 633-640 (1999).

36. M. Y. Galperin, Structural classification of bacterial response regulators: diversity of output domains and domain combinations. *J. Bacteriol.* **188**, 4169-4182 (2006).

37. E. J. Capra, M. T. Laub, The evolution of two-component signal transduction systems. *Annu. Rev. Microbiol.* **66**, 325-347 (2012).

38. P. Sehgal, C. Olesen, J. V. Møller, ATPase activity measurements by an enzyme-coupled spectrophotometric assay. *Methods in Mol. Biol.* **1377**, 105-109 (2016).

39. P. V. Konarev, V. V. Volkov, A. V. Sokolova, M. H. J. Koch, D. I. Svergun, PRIMUS – a Windows-PC based system for small-angle scattering data analysis. *J. Appl. Cryst.* **36**, 1277-1282 (2003).

40. D. I. Svergun, Determination of the regularization parameter in indirect-transform methods using perceptual criteria. *J. Appl. Cryst.* **25**, 495-503 (1992).

41. D. I. Svergun, Restoring low resolution structure of biological macromolecules from solution scattering using simulated annealing. *Biophys. J.* **76**, 2879-2886 (1999).

42. G. Ueno, K. Kanda, R. Hirose, K. Ida, T. Kumasaka, M. Yamamoto, RIKEN structural genomics beamlines at the SPring-8; high throughput protein crystallography with automated beamline operation. *J. Struct. Funct. Genomics* **7**, 15–22 (2006).

43. G. Ueno, H. Kanda, T. Kumasaka, M. Yamamoto, Beamline Scheduling Software: administration software for automatic operation of the RIKEN structural genomics beamlines at SPring-8. *J. Synchrotron Radiat.* **12**, 380–384 (2005).

44. G. Ueno, R. Hirose, K. Ida, T. Kumasaka, M. Yamamoto, Sample management system for a vast amount of frozen crystals at SPring-8. *J. Appl. Cryst*. **37**, 867–873 (2004).

45. Z. Otwinowski, W. Minor, Processing of X-ray diffraction data collected in oscillation mode. in *Methods in Enzymology* vol. 276 (ed. C. W. Carter, J. R. M. S.) 307-326 (Academic Press, New York) (1997).

46. M. Milani, L. Leoni, G. Rampioni, E. Zennaro, P. Ascenzi, M. Bolognesi, An active-like structure in the unphosphorylated StyR response regulator suggests a phosphorylation-dependent allosteric activation mechanism. *Structure* **13**, 1289-1297 (2005).

47. P. D. Adams, *et al.*, PHENIX: a comprehensive Python-based system for macromolecular structure solution. *Acta Cryst. D* **66**, 213-221 (2010).

48. P. Emsley, K. Cowtan, COOT: model-building tools for molecular graphics. *Acta Cryst. D* **60**, 2126-2132 (2004).

49. I. W. Davis, L. W. Murray, J. S. Richardson, D. C. Richardson, MOLPROBITY: structure validation and all-atom contact analysis for nucleic acids and their complexes. *Nucleic Acids Res.* **32**, W615-619 (2004).

50. A. Drozdetskiy, C. Cole, J. Procter, G. J. Barton, JPred4: a protein secondary structure prediction server. *Nucleic Acids Res.* **43**, W389-394 (2015).

51. A. Lupas, M. Van Dyke, J. Stock, Predicting coiled coils from protein sequences. *Science* **252**, 1162-1164 (1991).

52. J. Maupetit, P. Derreumaux, P. Tufféry, PEP-FOLD: an online resource for de novo peptide structure prediction. *Nucleic Acids Res.* **37**, W498-503 (2009).

53. D. Schneidman-Duhovny, M. Hammel, J. A. Tainer, A. Sali, Accurate SAXS profile computation and its assessment by contrast variation experiments. *Biophys. J.* **105**, 962-974 (2013).

54. A. T. Brünger, P. D. Adams, G. Marius Clore, W. L. DeLano, P. Gros, R. W. Grosse-Kunstlevee, J.-S. Jiang, J. Kuszewski, M. Nilges, N. S. Pannu, R. J. Read, L. M. Rice, T. Simonson, G. L. Warren, Crystallography & NMR System: a new software suite for macromolecular structure determination. *Acta Cryst.* D **54**, 905-921 (1998).

55. G. S. Wright, S. V. Antonyuk, S. S. Hasnain, A faulty interaction between SOD1 and hCCS in neurodegenerative disease. *Sci. Rep.* **6**, 27691 (2016).

56. C. Dominguez, R. Boelens, A. M. J. J. Bonvin, HADDOCK: a protein-protein docking approach based on biochemical and/or biophysical information. *J. Am. Chem. Soc.* **125**, 1731-1737 (2003).

57. B. Jiménez-Garcia, C. Pons, D. I. Svergun, P. Bernadó, J. Fernández-Recio, pyDOCKSAXS: protein-protein complex structure by SAXS and computational docking. *Nucleic Acids Res.* **43**, W356-361 (2015).

58. D. Schneidman-Duhovny, M. Hammel, J. A. Tainer, A. Sali, FoXS, FoXSDock and MultiFoXS: single-state and multi-state structural modeling of proteins and their complexes based on SAXS profiles. *Nucleic Acids Res.* **44**, W424-429 (2016).

Acknowledgments: Thanks to Synchrotron Soleil and SPring-8 for the provision of SAXS facilities. The authors acknowledge the support and the use of resource of instruct, a landmark ESFRI project (iNEXT 2822). **Funding:** This work was supported by the Fumi Yamamura Memorial Foundation for Female Natural Scientists from Chuo Mitsui Trust and Banking (H.S.), Hyogo Science and Technology Association (H.S.), RIKEN Pioneering Project "Integrated Lipidology" (H.S.) and "Molecular System" (Y.S.), and JSPS KAKENHI Grant Numbers JP26220807 (Y.S. and H.S.), JP25871213 (H.S.). **Author contributions:** G.S.A.W., S.V.A., S.S.H., Y.S. and H.S. designed this study. A.S., H.Nakamura and H.S. created the systems for expressing recombinant FixL and FixJ in *E. coli*. T.Hikima and M.Y. installed SEC-SAXS system at BL45XU in SPring-8. G.S.A.W., A.S., Y.N. and H.S. purified FixL and FixJ samples. H.S. prepared the expression systems for FixL mutants. M.K. purified FixL mutant proteins and measured their phosphotransfer activities. K.N. and H.Nishitani performed autophosphorylation activity assay using γ-^{32}P-ATP. H.S. performed phosphatase activity assay by Phos-tag SDS-PAGE. G.S.A.W., A.S., T.Hikima and H.S. measured and analyzed SAXS data. G.S.A.W. modeled the pseudo-atomic structures. Y.N. crystallized FixJ. Y.N. and T.Hisano collected, processed and refined the crystal data. G.S.A.W., T.Hisano, S.V.A., S.S.H., Y.S. and H.S. wrote the manuscript. All authors analyzed data and discussed the results. **Competing interests:** The authors declare that they have no competing interests. **Data and materials availability:** All data needed to evaluate the conclusions in the paper are present in the paper and/or the Supplementary Materials. The atomic coordinates and structure factors for FixJ (PDB IDs: 5XSO and 5XT2) have been deposited in the PDB (http://www. wwpbd.org). The SAXS measurements at SPring-8 BL45XU were performed under proposals 20140099, 20150017, 20160015, 20170092. The X-ray diffraction measurements were performed at SPring-8 BL26B2 (Proposals 20160015).

TABLES

Table 1. Phospho-transfer activities of full-length FixL to FixJ by ATP-NADH coupled assay (*38*).

State of heme in FixL [Activity]	Specific activity (nmoles/min./mg)[#]
Deoxy (Fe^{2+}) [Active]	108±4
Oxy (Fe^{2+}-O_2)[§] [Inactive]	43±5
Met (Fe^{3+}) [Active]	122±6
Cyanomet (Fe^{3+}-CN^-) [Inactive]	12±2

[#]The initial rates were obtained from the time courses for the formation of phosphorylated FixJ. These values were calculated from more than three independent time course experiments. [§]Oxy FixL was prepared to bind O_2 in air to prevent fast autoxidation. This sample contained *ca.* 30% of deoxy form by the low O_2 affinity, which was consistent with a previous report (*8*). Due to the contaminated deoxy FixL, the activity became higher even in the inactive state.

Table 2. Structural parameters for FixL and FixL/FixJ complex determined by SEC-SAXS experiments at BL45XU in SPring-8.

Sample	Guinier R_g (Å)	D_{max} (Å)	Porod volume V_p (Å^3)	Molecular mass from V_p (kDa)
Met FixL	49.7±0.1	163±4	224,220±3,061	140.1±1.9
Cyanomet FixL[*]	48.4±0.2	158±3	218,075±3,693	136.3±2.3
Truncated FixL[§]	34.0	121	100,790	63.0
FixJ	22.3±0.2	66±2	39,230±1,115	24.5±0.7
Met FixL-FixJ complex	53.1±0.1	160±5	296,970±2,478	185.4±1.5
Cyanomet FixL-FixJ complex	52.1±0.1	163±3	273,820±2,253	171.1±1.4
Met FixL-$FixJ_N$ complex	48.9±0.1	170±3	245,753±2,306	153.6±1.4

*The data collection was performed using KCN-containing buffer [40 mM Tris/HCl (pH8.0), 10%(w/v) glycerol, 5 mM potassium cyanide, 5 mM $MgCl_2$]. [§]The parameters for truncated FixL were obtained by one measurement. Other samples were analyzed from multiple measurements (N>3).

Figures

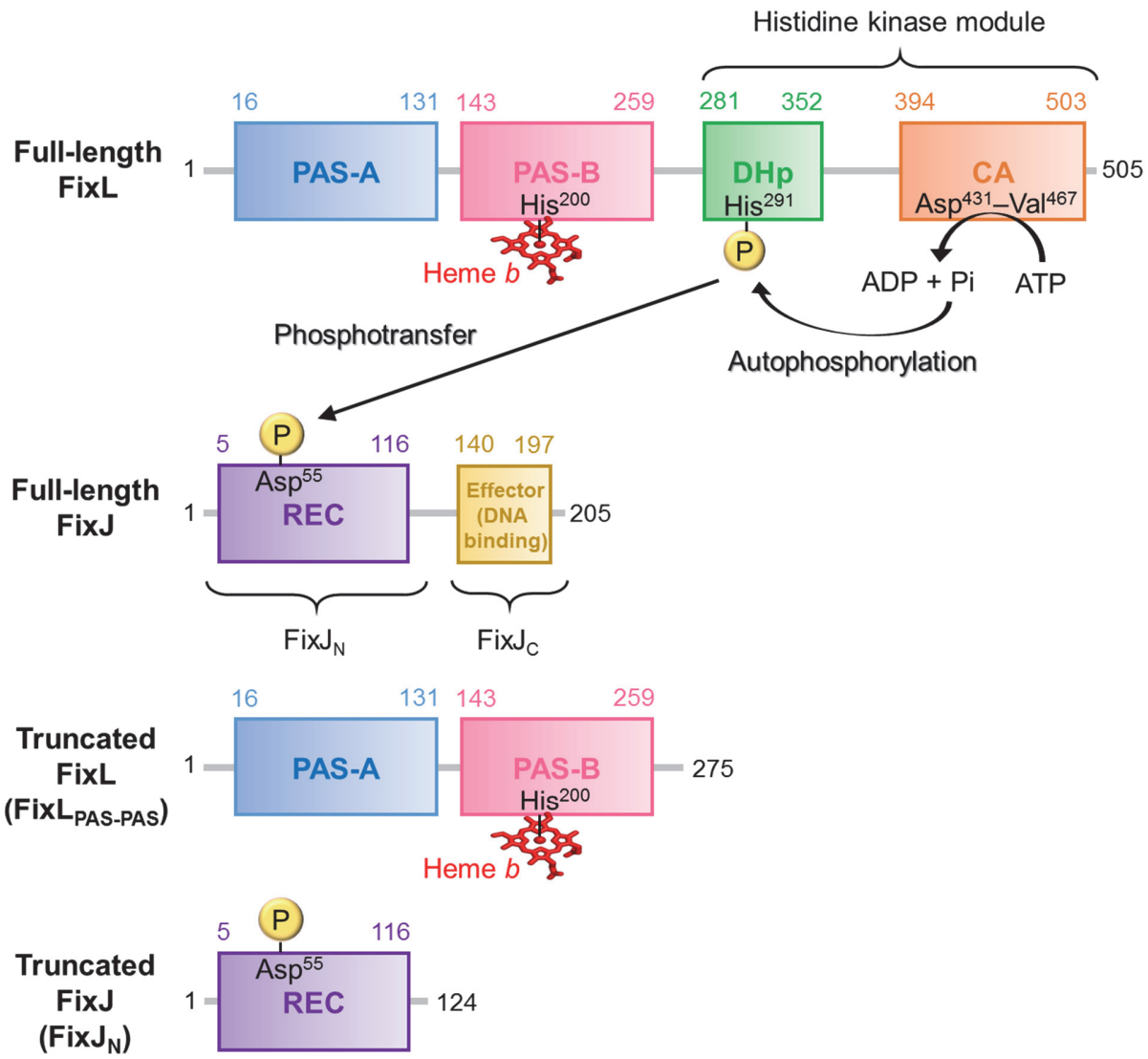

Fig. 1. Schematic representation of the domain structures of full-length and truncated versions of *B. japonicum* FixL and FixJ. Full-length *B. japonicum* FixL comprises two N-terminal PAS domains, PAS-A and PAS-B, and C-terminal dimerization and histidine phosphotransfer (DHp) and catalytic ATP-binding (CA) domains. His^{200} in the PAS-B domain is critical for binding to heme; His^{291} in the DHp domain is the site of autophosphorylation; and Asp^{431}-Val^{467} of the CA domain constitutes the ATP binding site. Full-length *B. japonicum* FixJ contains an N-terminal receiver (REC) domain and a C-terminal effector domain that binds to DNA. FixJ is activated by FixL-mediated phosphorylation at Asp^{55}. Structures of the truncated FixL and FixJ proteins $FixL_{PAS-PAS}$ and $FixJ_N$ used in this study are indicated. The residues that define the boundaries of these domains are noted. Domain structures were generated using the SMART tool (http://smart.embl-heidelberg.de/).

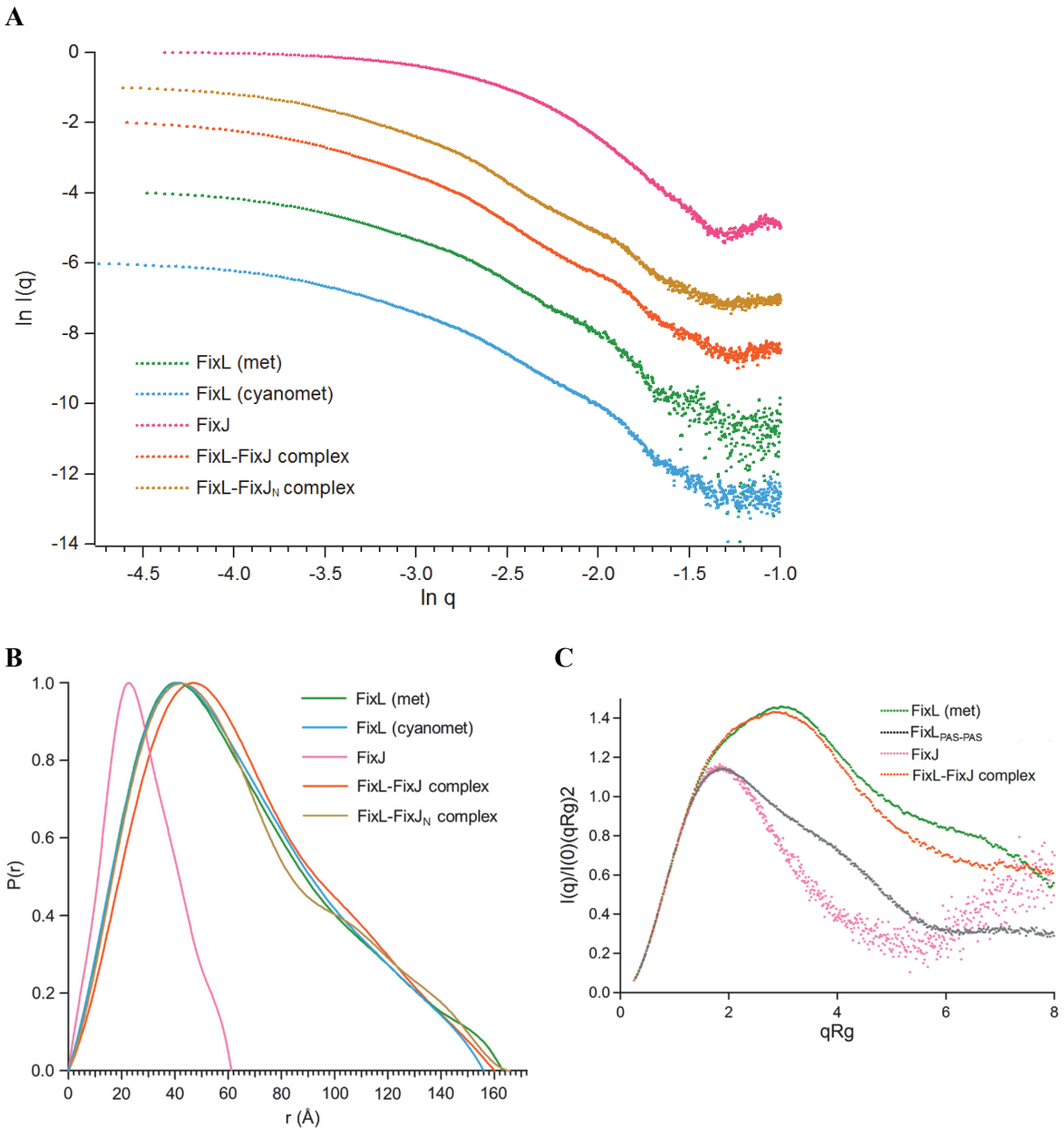

Fig. 2. SEC-SAXS profiles of full-length FixL, FixJ, and FixL-FixJ complexes. (**A**) Log-log plots of met and cyanomet forms of full-length FixL, full-length FixJ, the FixL-FixJ complex, and the FixL-FixJ$_N$ complex scattering. (**B**) Corresponding pair distance distribution functions. (**C**) Dimensionless Kratky plots, which compare the compactness of a protein, for full-length FixL (met form), truncated FixL$_{PAS-PAS}$ form of FixL (met form), full-length FixJ, and the full-lengths FixL and FixJ complex. A compact protein has a peak maximum at √3 and 1.2. Movement of the peak into the positive quartile indicates unfolding and conformational flexibility. Data was collected on the BL45XU beamline at the SPring-8 synchrotron. N>3 from independent protein preparations and data collections.

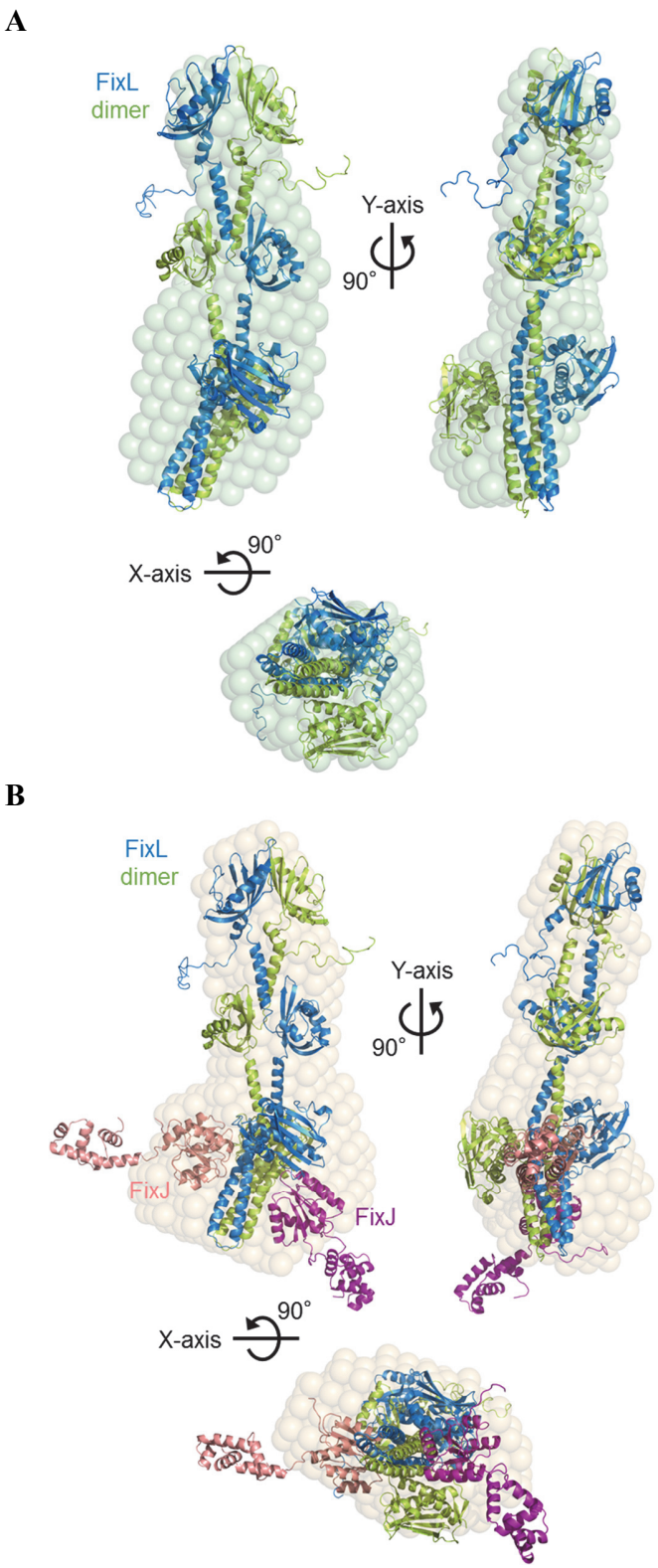

Fig. 3. Space filling and pseudo-atomic models of full-length FixL and the FixL-FixJ complex. SAXS models of (**A**) the met form of full-length FixL and (**B**) the FixL-FixJ complex showing the overall shape, domain arrangement and mode of complexation. The FixJC effector domain is invisible in the *ab initio* model of the FixL-FixJ complex because it does not form part of the complex interface and is allowed conformational freedom by its inter-domain linker as characterized in Fig. 4.

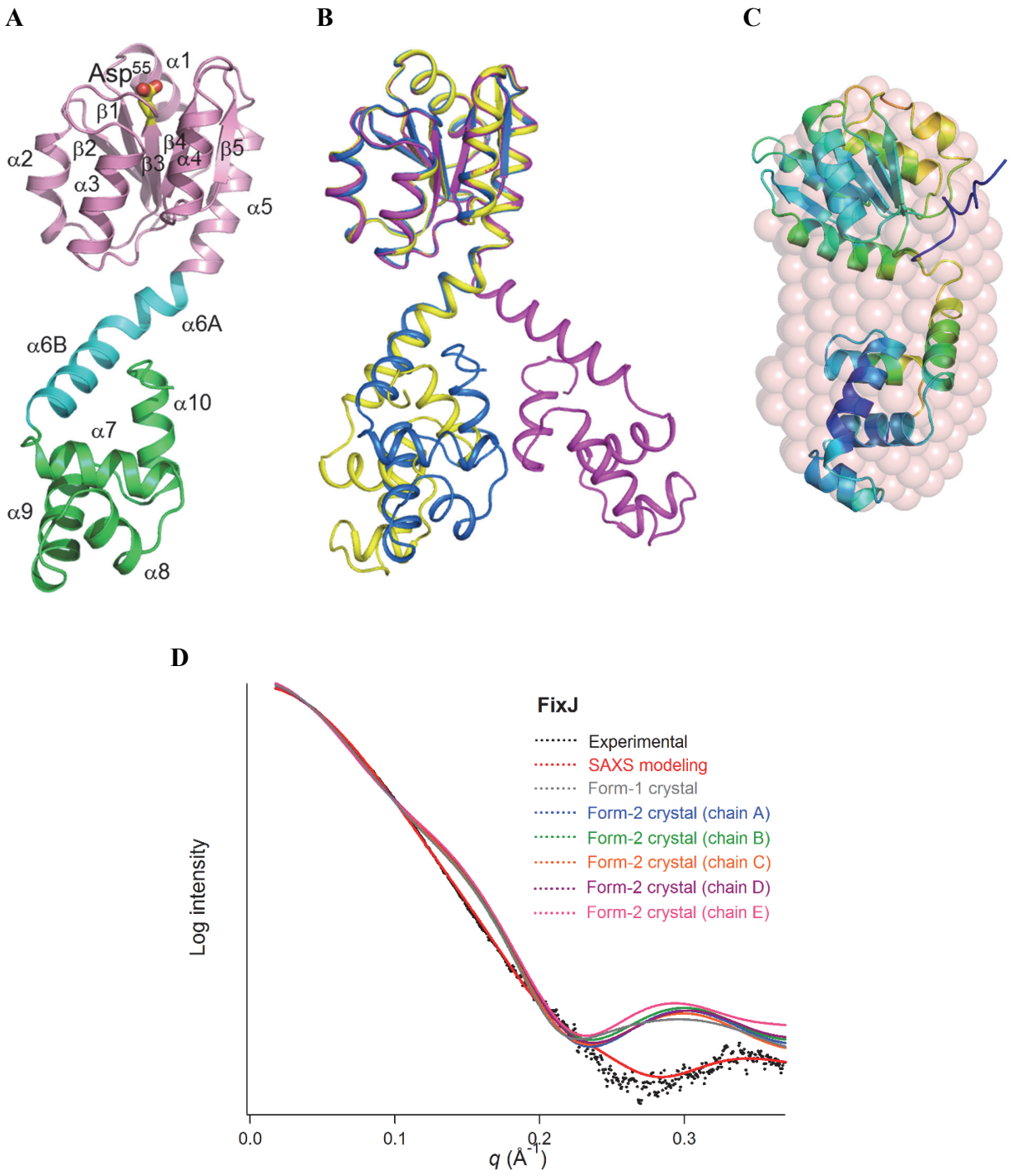

Fig. 4. Crystal and SAXS solution structures of full-length FixJ. (**A**) Crystal structure of full-length FixJ showing the relative positions of the N-terminal (pink), linker (cyan), and C-terminal (green) domains. The phosphorylation site, Asp^{55}, is indicated as a stick model (carbon and oxygen atoms are indicated in yellow and red, respectively). (**B**) Comparison of crystal structures of FixJ in space groups $C222_1$ (blue) and $P2_12_12_1$ [yellow (chain A) and magenta (chain E)]. This view is rotated by 90° compared to (A). (**C**) Space filling and pseudo-atomic models of full-length FixJ. (**D**) Comparison of FixL crystallographic and SAXS models against experimental SAXS data.

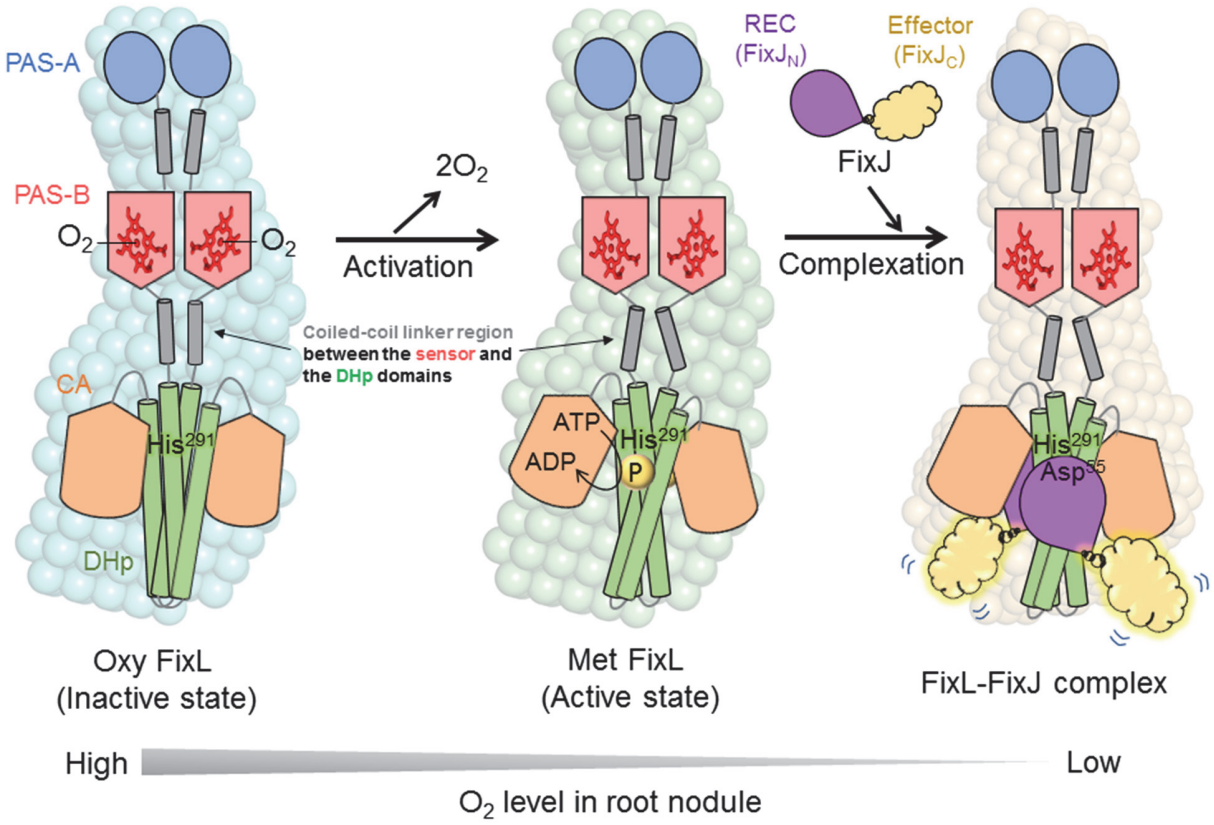

Fig. 5. Schematic representation of of the FixL/FixJ TCS. Our SAXS results suggest that there are no large overall changes of the shape of full-length FixL upon O_2 dissociation from the heme group. However, the orientation of the coiled-coil helices between the heme-containing PAS-B (pink) and DHp (green) domains may change. Such localized structural change could alter the distance between the ATP binding site in the CA domain (orange) and the autophosphorylation site at His^{291}. In the full-length FixL-FixJ complex, a phosphorylation site (Asp^{55}) in the FixJ REC domain approaches to the His^{291} of the FixL DHp domain, while the C-terminal DNA binding domains of FixJ exhibit multiple-conformation due to flexible linker conformation.

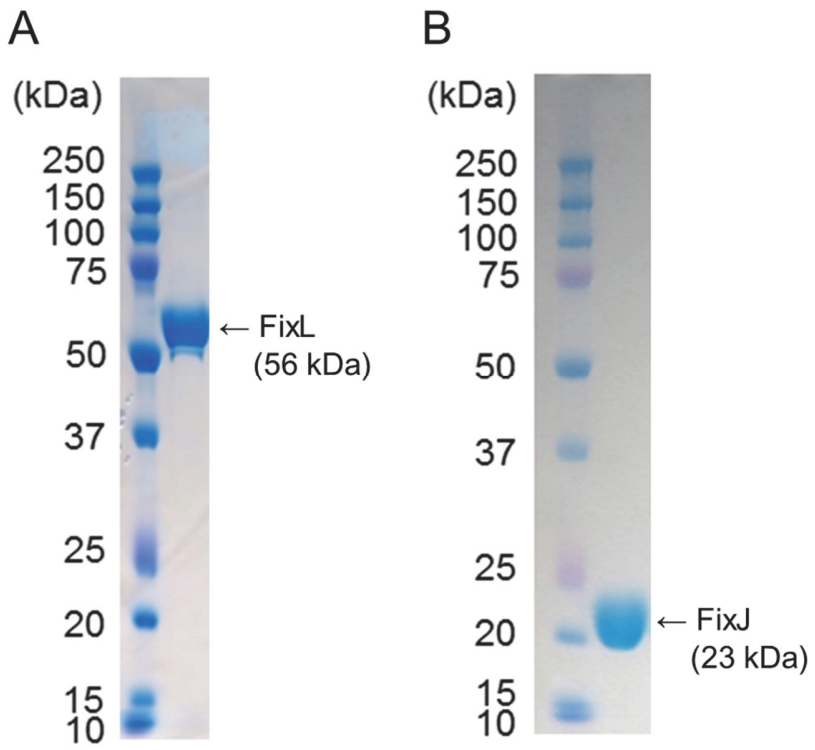

figure S1. 10% SDS-PAGE of purified FixL (A) and FixJ (B) proteins. The leftmost lane on each gel is Precision Plus Protein^{TM} Dual Color Standards (BIO-RAD), another lane is protein loaded. The purified samples were mixed with 2 x SDS-PAGE buffer containing 125 μM Tris/HCl pH6.8, 4% SDS, 20% w/v sucrose, 0.01% w/v BPB, 10% v/v 2-mercaptoethanol, and boiled at 95 ºC for 10 mins before the electrophoresis. 10% NuPAGE Bis-Tris gels (Thermo Fisher Scientific) was used for the electrophoresis with NuPAGE MOPS SDS running buffer (ThermoFisher Scientific) for FixL and NuPAGE MES SDS running buffer (ThermoFisher Scientific) for FixJ. The gels were stained by EzStain AQua (ATTO).

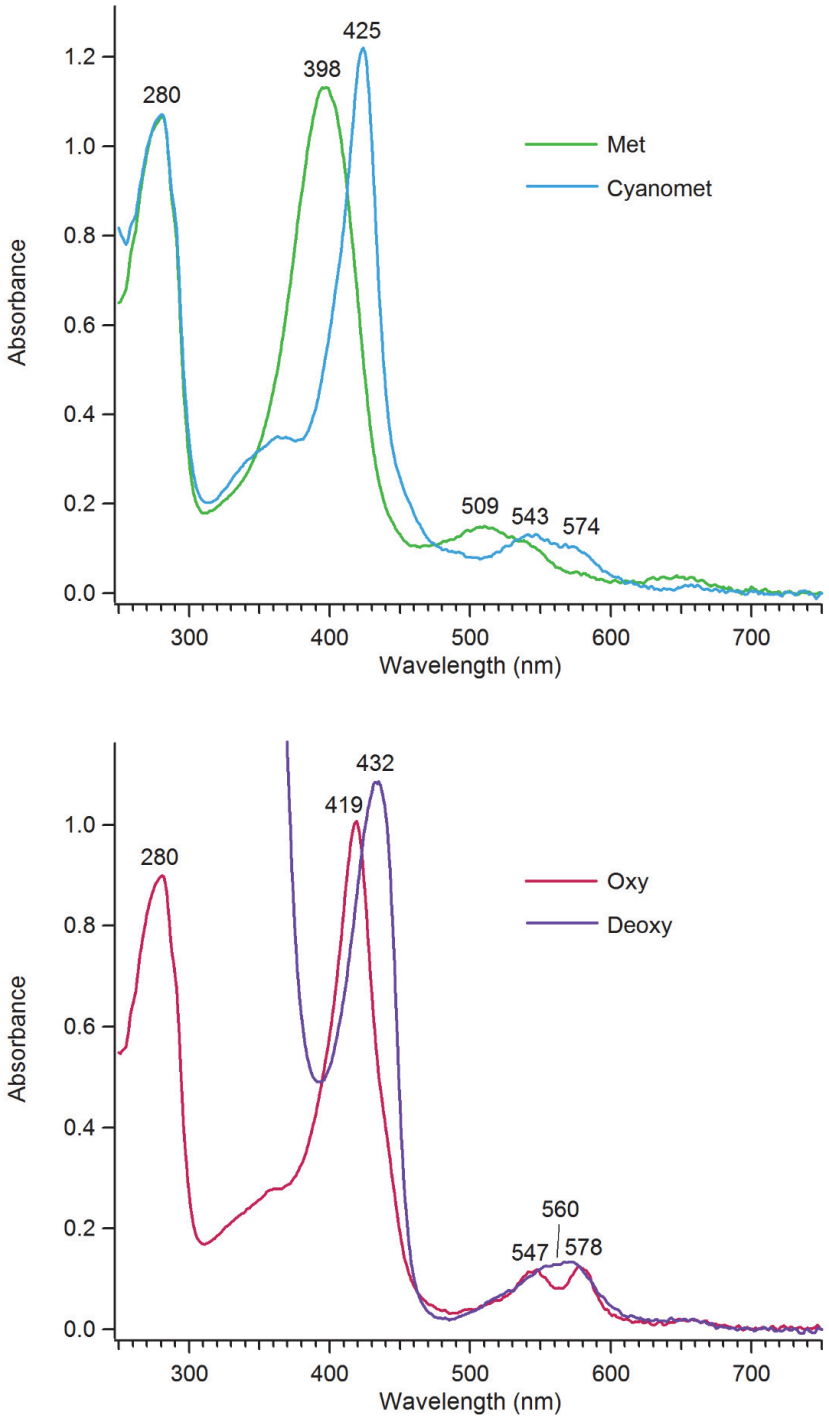

figure S2. Optical absorption spectra of full-length FixL in oxy, deoxy, met and cyanomet forms. These spectra were measured in 40 mM Tris/HCl (pH8.0), 150 mM NaCl, 10% (w/v) glycerol at 20 ºC by NanoDrop™ 2000c spectrophotometers (ThermoFisher Scientific).

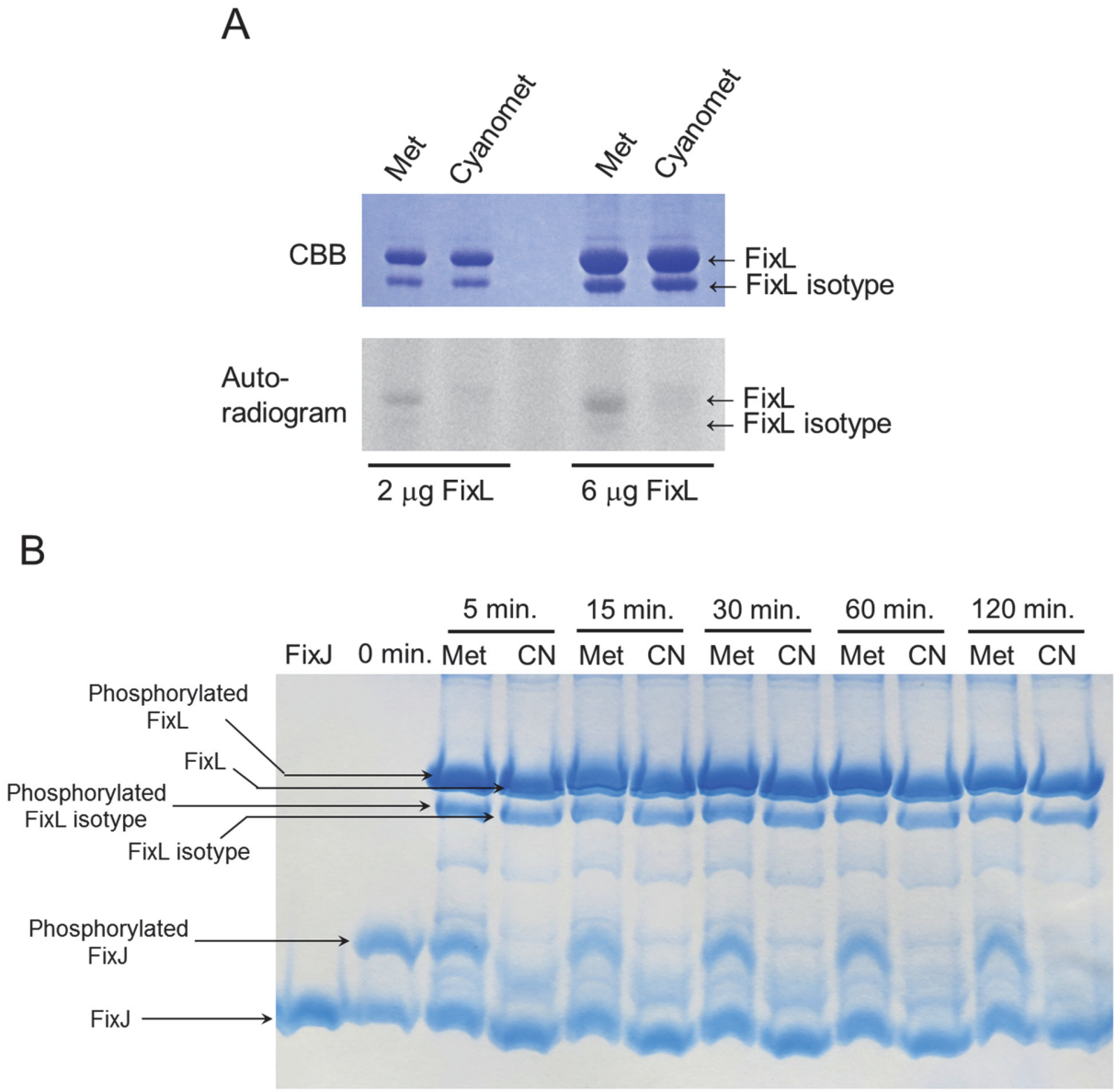

figure S3. Assay of autophosphorylation (A) and phosphatase activity (B) of FixL.
(A) Autophosphorylation activity of the roughly purified FixL in the met and cyanomet forms. CBB stained protein bands on a SDS-PAGE gel are on the top panel. The extra bands on the bottom of the main bands are undenatured FixL isotype. The bottom panel is overexposed autoradiogram of the same gel. (B) Acetylphosphorylated FixJ was prepared by the addition of 50 mM acetyl phosphate lithium potassium salt (Sigma-aldrich) to 20 μM FixJ in 50 mM Tris/HCl pH8.0, 50 mM KCl, 1 mM $MgCl_2$, 50 μM $MnCl_2$, and incubated at 23 ºC for 2 hours. 15% Zn^{2+}-Phos-tag SDS-PAGE containing 50 μM Phos-tag® acrylamide (Wako) and 100 μM $ZnCl_2$. Tris-Glycine buffer was used for the electrophoresis.

A

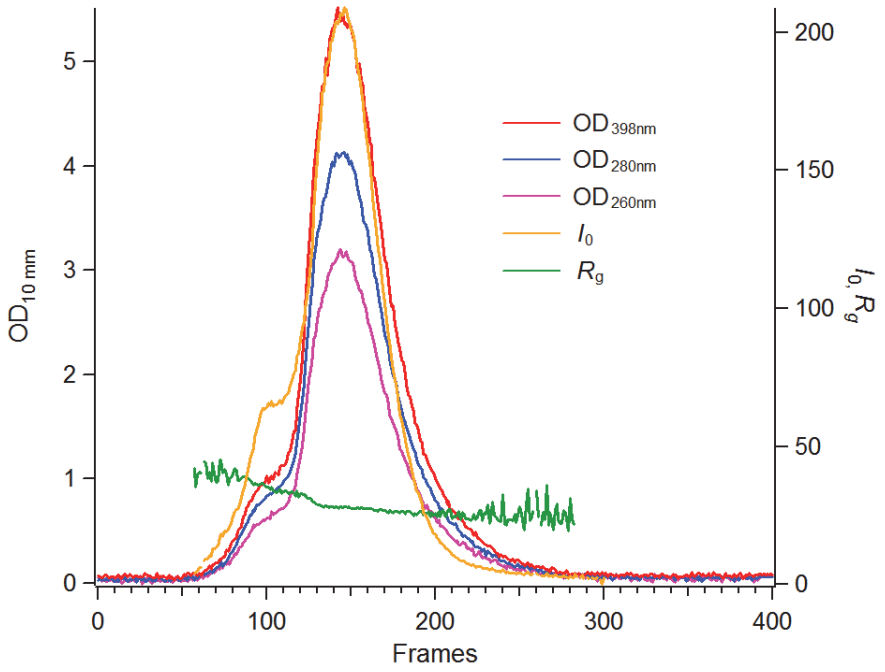

B

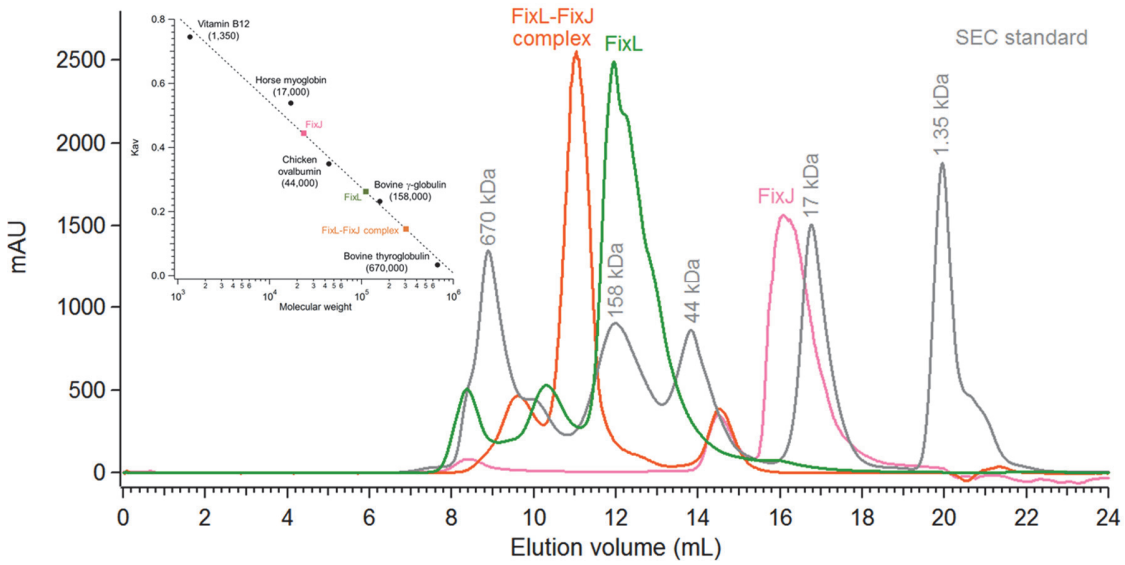

figure S4. SEC profiles. (A) Met FixL protein elution at BL45XU in SPring-8 monitored by UV/visible spectroscopy and SAXS parameters: OD_{398nm}, OD_{280nm}, OD_{260nm}, I_0 and R_g, which were automatically calculated using PRIMUS (*33*). For the data analysis, we selected the data highlighted in grey. (B) FixL-FixJ complex formation was checked by SEC elution position change. SEC was performed on Superdex200 Increase 10/300 (GE healthcare) using the same buffer with SEC-SAXS measurements (40 mM Tris/HCl pH8.0, 10% w/v glycerol, 5 mM $MgCl_2$ for FixL or FixJ, and the buffer containing 100 mM FixJ for FixL-FixJ complexation). For molecular weight estimation, a calibration curve of K_{av} versus log molecular weight (inset, dotted line) was prepared using a commercially available gel filtration standard (BIO-RAD). Calculation of the K_{av} values were used $K_{av} = (V_e - V_o)/(V_c - V_o)$, where V_o = column void volume, V_e = elution volume at the peak, and V_c = geometric column volume. The calibration curve provided an equation of $Y = -0.267 \log X + 1.608$ to estimate the molecular weight (X) of FixL, FixJ, and their complex using Y (K_{av}) values.

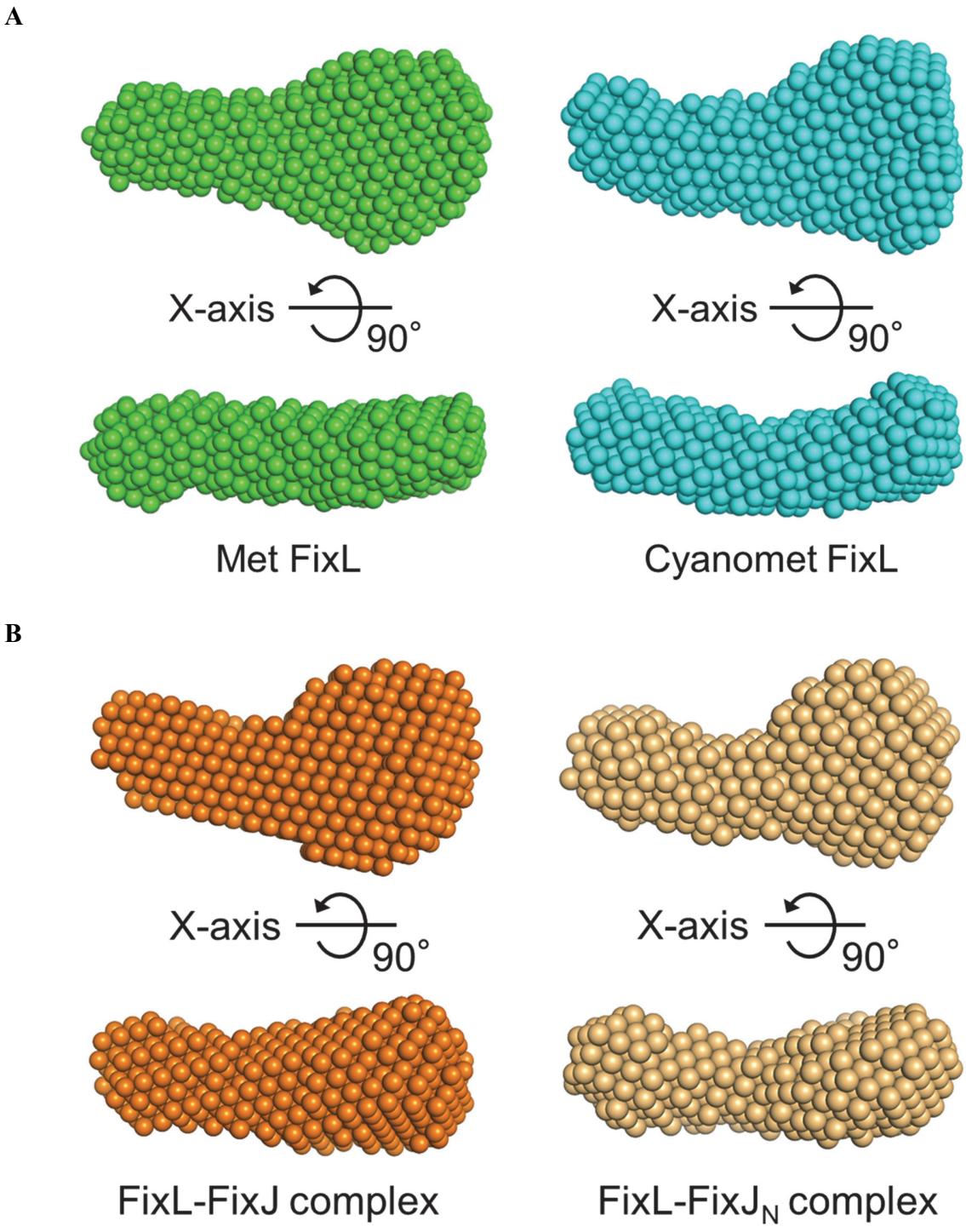

figure S5. Space filling models of FixL protein and its complex with FixJ or FixJ$_N$. (A) met and cyanomet forms, (B) full-length FixL-FixJ and FixL-FixJ$_N$ complexes.

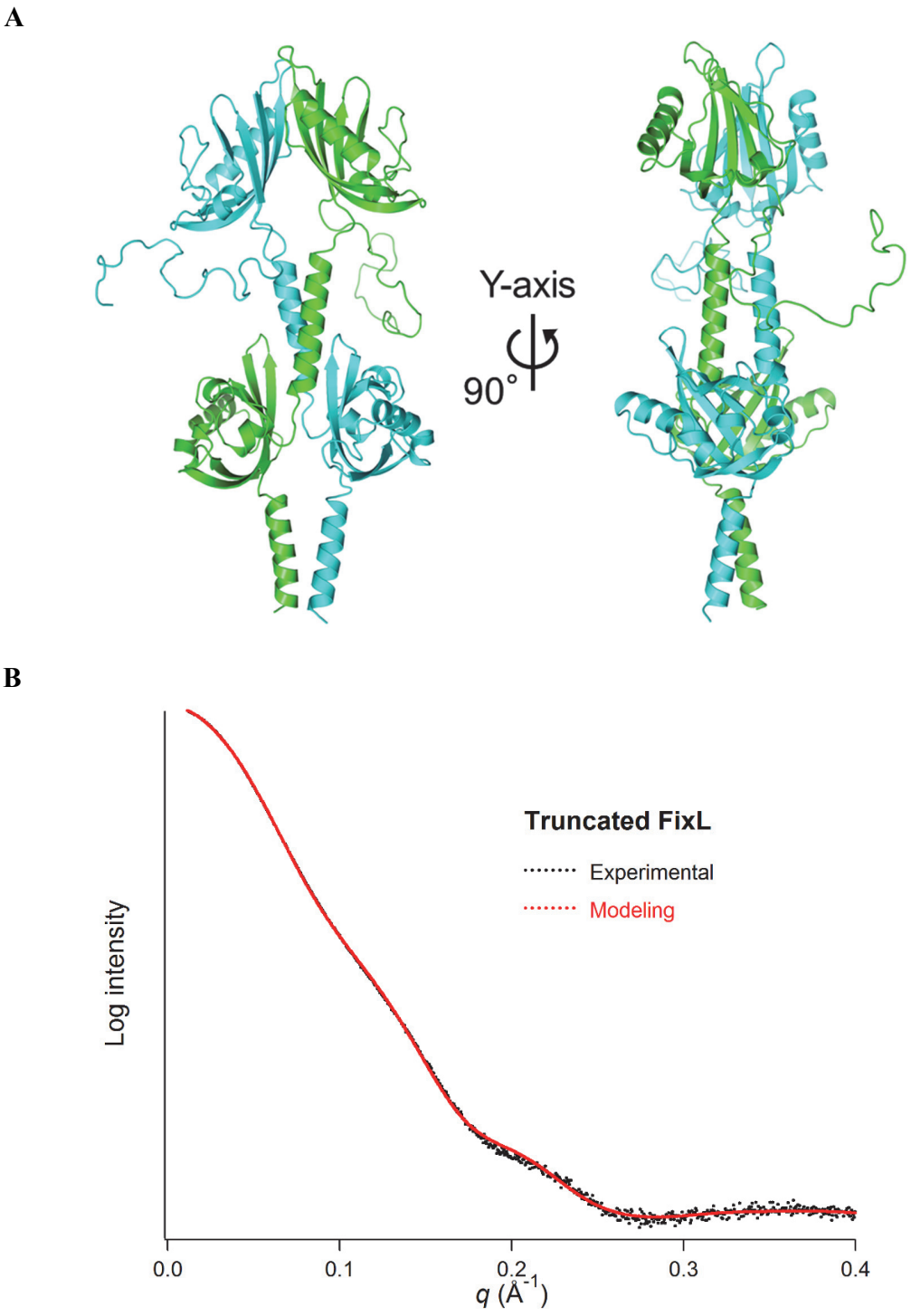

figure S6. Pseudo-atomic model and SAXS curve of truncated FixL ($FixL_{PAS-PAS}$). (A) Domain arrangement of truncated FixL containing PAS-A and PAS-B domains. The PAS-A and PAS-B structure is identical to that found within the full-length FixL molecule and shows (B) a very good fit to the experimental data.

A

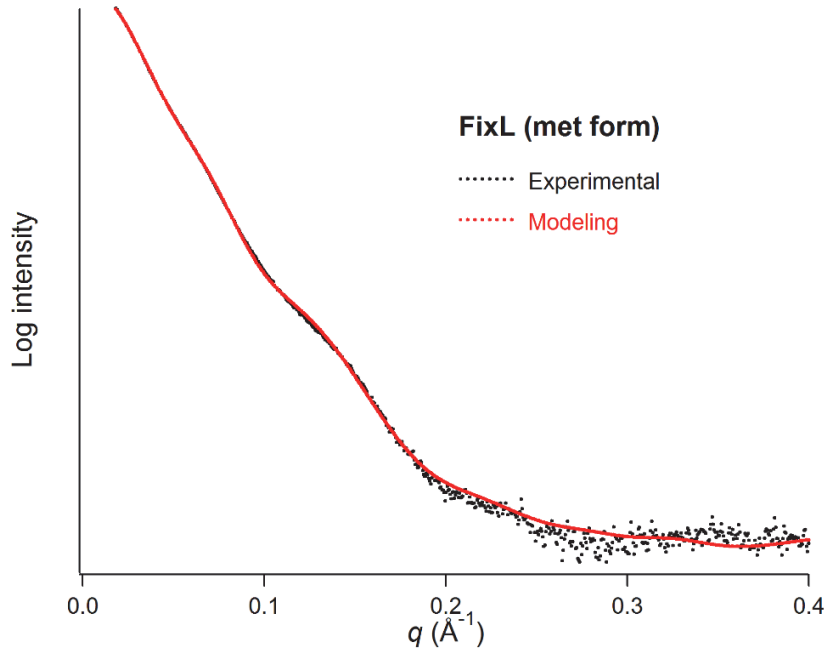

B

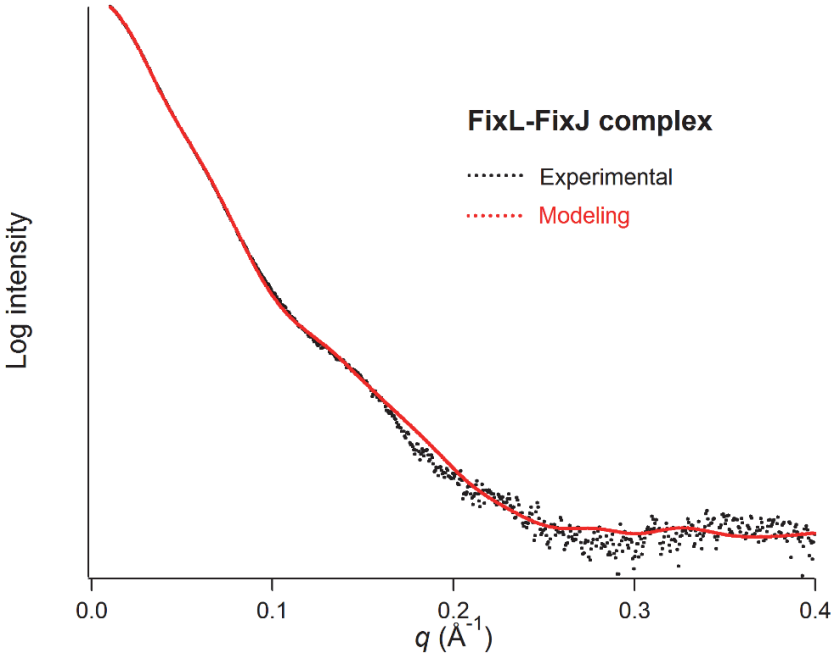

figure S7. Experimental and simulated SAXS curves of FixL in the met form (A) and FixL-FixJ complex (B). The χ values of the curve fitting are 2.57 and 2.71, respectively.

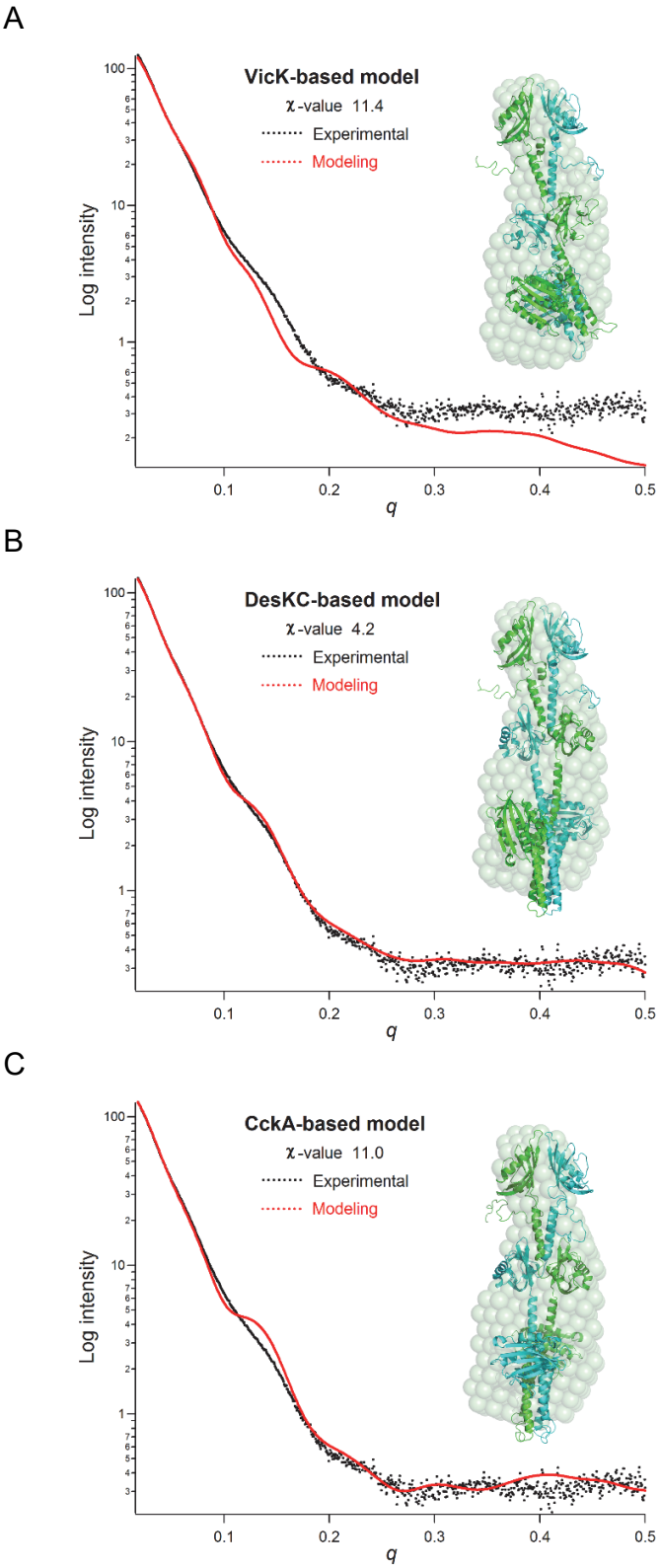

figure S8. SAXS curves and pseudo-atomic models of full-length FixL based on the YF1 blue light receptor compared with other models based on symmetric DHp domain structures. The histidine kinase modules of VicK (PDB ID: 5IDJ), DesKC (PDB ID: 5IDJ) and CckA (PDB ID: 5IDJ) could be used as templates for FixL but yielded poorer correlation with the experimental SAXS data: χ 11.4, 4.2 and 11.0 respectively in comparison with 2.57 for YF1-based FixL.

A

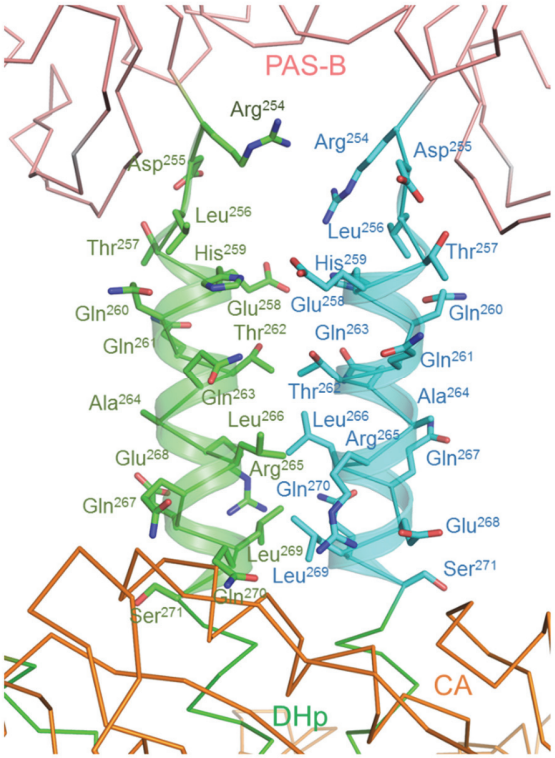

B

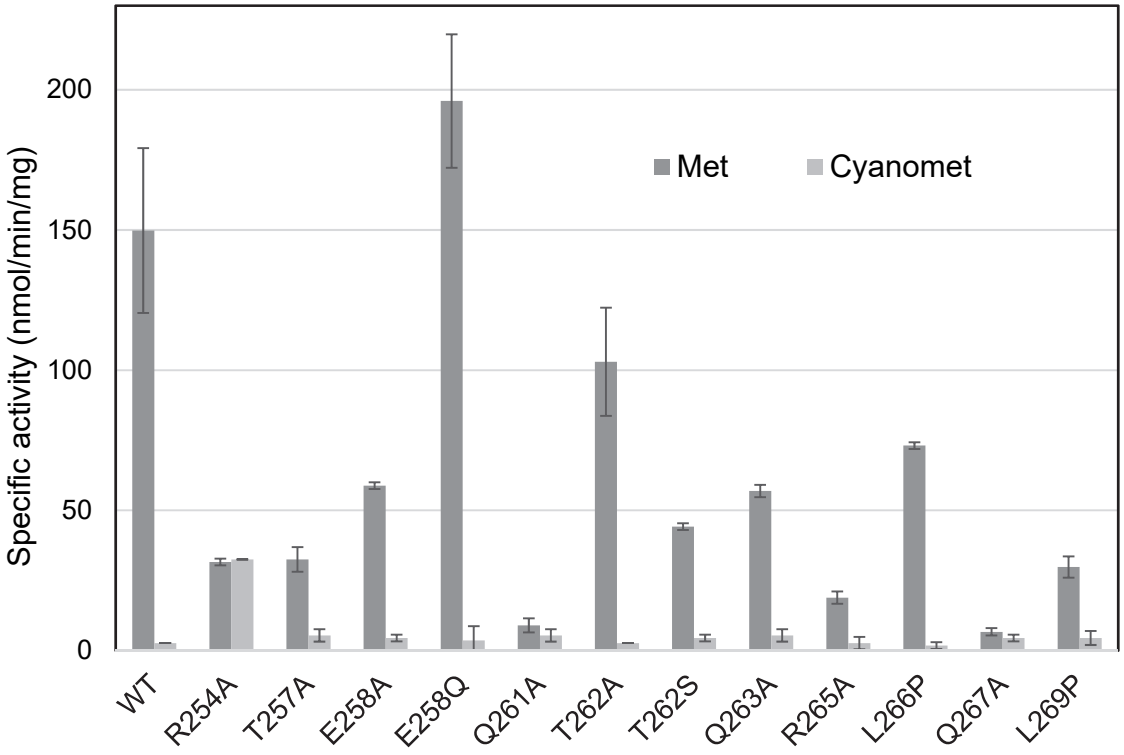

figure S9. Phosphorylation activities of FixL mutants on the coiled-coil region between PAS-B and DHp domains. (A) Position of amino acid residues on the coiled-coil helices in the YF-1-based pseudo-atomic FixL model. The helix in chain-A and -B represent in green and cyan, respectively, (B) Phosphotransfer activity from full-length His-tagged WT and mutants FixL to FixJ measured by ATP-NADH coupled assay.

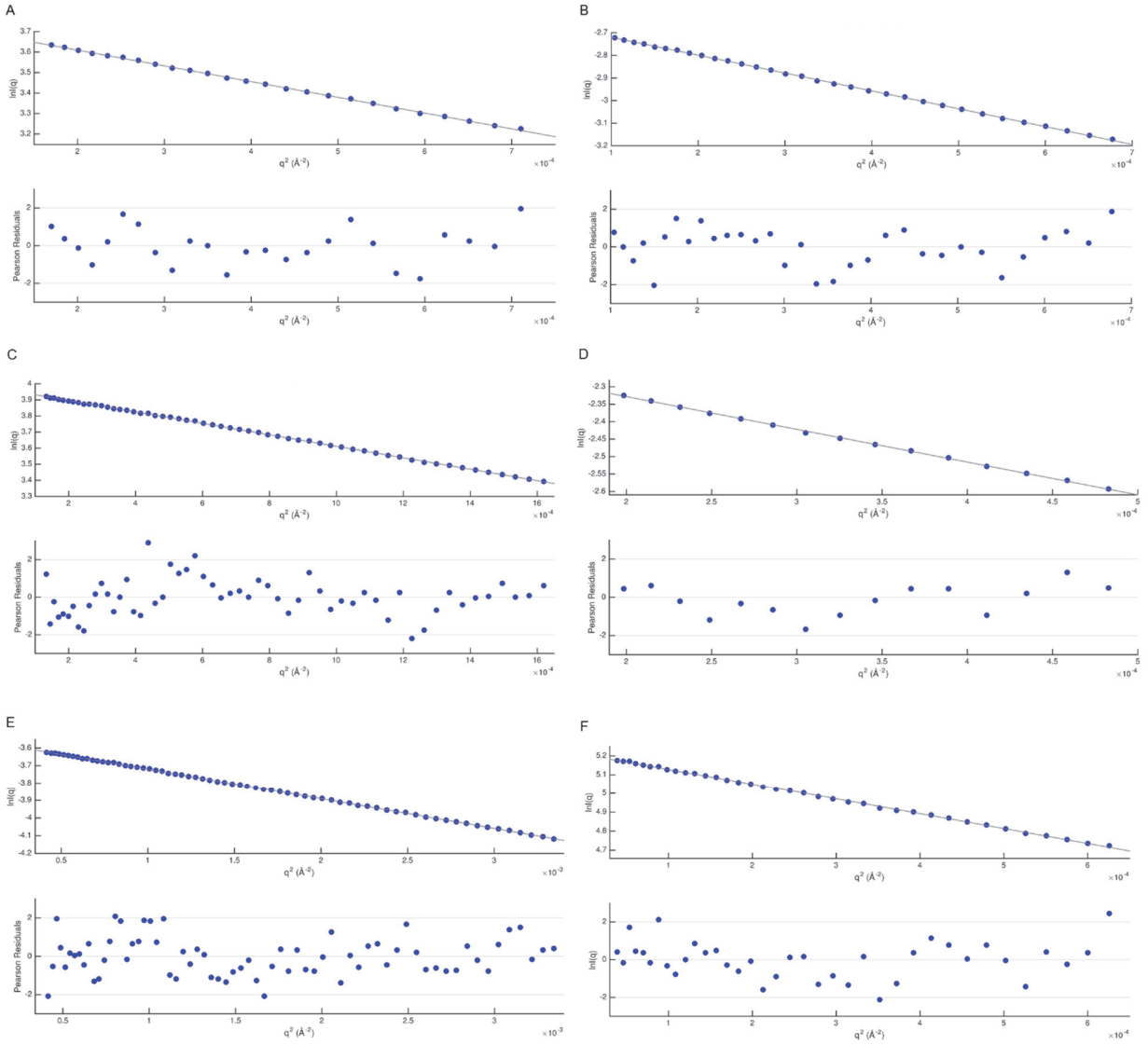

figure S10. Guinier plots (upper panels) with Pearson residuals (lower panels) of (A) full-length met FixL, (B) full-length cyanomet FixL, (C) truncated FixL ($FixL_{PAS-PAS}$), (D) full-lengths FixL and FixJ complex, (E) full-length FixJ, and (F) truncated FixJ ($FixJ_N$) on SEC-SAXS experiments.

table S1. Structural parameters for FixL and FixJ determined by static SAXS experiment at BL45XU in SPring-8.

Sample	I_0 (Å)	Guinier R_g (Å)	D_{max} (Å)	Porod volume V_p (Å^3)	Molecular mass from V_p (kDa)
Met FixL	26.2	54.9	205	224,410	140.2
Cyanomet FixL	20.9	51.0	195	193,200	120.7
FixJ	49.6	21.1	69	41,320	25.8

table S2 Structural parameters for FixL and FixJ determined by SEC-SAXS experiment at SWING beamline in SOLEIL. Standard deviation stated where more than three measurements were done.

Sample	Guinier R_g (Å)	D_{max} (Å)	Porod volume V_p (Å^3)	Molecular mass from V_p (kDa)
Met FixL	49.4±0.8	169±4.3	215,120±135	134.5±0.08
Cyanomet FixL	49.2±0.9	167±1.5	218,400±136	136.5±0.09
FixJ	22.5	58.5	39,189	24.5
Met FixL-FixJ complex	53.6	211	281,348	175.8

table S3 Crystallographic statistics of FixJ.

	Form 1[a]	Form 2[b]
PDB code	5XSO	5XT2
Data collection		
Beamline	BL26B2	BL26B2
Space group	$C222_1$	$P2_12_12_1$
Cell dimensions		
a, *b*, *c* (Å)	70.9, 79.3, 120.1	76.7, 137.9, 142.3
Resolution (Å)	39.7 – 1.78 (1.81 – 1.78)	49.5 – 2.65 (2.70 – 2.65)
R_{sym} (%)	0.055 (0.832)	0.061 (1.127)
R_{meas} (%)	0.056 (0.872)	0.062 (1.161)
$I / \sigma(I)$	45.8 (1.9)	60.3 (2.0)
Completeness (%)	99.5 (93.5)	99.6 (95.1)
Redundancy	14.3 (9.9)	28.2 (17.4)
Wilson *B* (Å^2)	16.6	33.5
Refinement		
No. of reflections	31,438	41,530
R_{work} / R_{free}	0.171 / 0.204	0.206/0.248
No. of atoms		
Protein	1,567	7,509
Ligand/ion	42	74
Water	257	163
B-factors (Å^2)		
Protein	29.6	51.1
Ligand/ion	42.7	60.2
Water	41.8	37.1
Coordinate error (Å) †		
r.m.s. deviations		
Bond lengths (Å)	0.016	0.013
Bond angles (°)	1.27	1.35
Ramachandran plot (%)		
Preferred	98.0	97.4
Allowed	0	2.6
Outlier	0	0

[a]Crystallized in space group $C222_1$ by vapour diffusion against mother liquor containing 10%(w/v) PEG8000, 10%(w/v) PEG1000, 0.8 M sodium formate, 20%(v/v) glycerol, and 0.1 M Tris-HCl (pH 7.5). [b]Crystallized in space group $P2_12_12_1$ by vapour diffusion against a mother liquor containing 20%(w/v) pentaerythritol ethoxylate (15/4 EO/OH), 0.1 M magnesium formate, 20%(v/v) glycerol, and 0.1 M Tris-HCl (pH 8.5).